REPORT DOCUMENTATION PAGE

Form Approved
OMB No. 0704-0188

1. REPORT DATE *(DD-MM-YYYY)*	2. REPORT TYPE	3. DATES COVERED *(From - To)*
14-03-2011	Final Report	22/01/2008-21/01/2011

4. TITLE AND SUBTITLE
Application of the Oriented-Eddy Collision Model to Complex Turbulent Flows

5a. CONTRACT NUMBER

5b. GRANT NUMBER
N00014-08-1-0275

5c. PROGRAM ELEMENT NUMBER

6. AUTHOR(S)
Blair Perot

5d. PROJECT NUMBER
08PR03418-00

5e. TASK NUMBER

5f. WORK UNIT NUMBER

7. PERFORMING ORGANIZATION NAME(S) AND ADDRESS(ES)
University of Massachusetts, Amherst
70 BUTTERFIELD TERRACE
AMHERST, MA 01003-9333

8. PERFORMING ORGANIZATION REPORT NUMBER

9. SPONSORING/MONITORING AGENCY NAME(S) AND ADDRESS(ES)
Office of Naval Research
875 North Randolph Street
Arlington, VA 22203-1995

10. SPONSOR/MONITOR'S ACRONYM(S)
ONR

11. SPONSOR/MONITOR'S REPORT NUMBER(S)

12. DISTRIBUTION/AVAILABILITY STATEMENT

13. SUPPLEMENTARY NOTES

14. ABSTRACT
Describes a new approach to turbulence modeling, involving the modeling of turbulence as a collection of interacting oriented eddies. The model was implemented in a open source CFD framework, OpenFoam. The model was tested on complex turbulent flows involving no slip surfaces and system rotation.

15. SUBJECT TERMS
Turbulence Modeling

16. SECURITY CLASSIFICATION OF:			17. LIMITATION OF ABSTRACT	18. NUMBER OF PAGES	19a. NAME OF RESPONSIBLE PERSON
a. REPORT	b. ABSTRACT	c. THIS PAGE			Blair Perot
Not classifiec	Not classifiec	Not Classifie	None	62	19b. TELEPHONE NUMBER *(Include area code)* 413-545-3925

DEFENSE TECHNICAL INFORMATION CENTER

Information for the Defense Community

DTIC® has determined on 3/23/2011 that this Technical Document has the Distribution Statement checked below. The current distribution for this document can be found in the DTIC® Technical Report Database.

☒ **DISTRIBUTION STATEMENT A.** Approved for public release; distribution is unlimited.

☐ **© COPYRIGHTED.** U.S. Government or Federal Rights License. All other rights and uses except those permitted by copyright law are reserved by the copyright owner.

☐ **DISTRIBUTION STATEMENT B.** Distribution authorized to U.S. Government agencies only (fill in reason) (date of determination). Other requests for this document shall be referred to (insert controlling DoD office).

☐ **DISTRIBUTION STATEMENT C.** Distribution authorized to U.S. Government Agencies and their contractors (fill in reason) (date determination). Other requests for this document shall be referred to (insert controlling DoD office).

☐ **DISTRIBUTION STATEMENT D.** Distribution authorized to the Department of Defense and U.S. DoD contractors only (fill in reason) (date of determination). Other requests shall be referred to (insert controlling DoD office).

☐ **DISTRIBUTION STATEMENT E.** Distribution authorized to DoD Components only (fill in reason) (date of determination). Other requests shall be referred to (insert controlling DoD office).

☐ **DISTRIBUTION STATEMENT F.** Further dissemination only as directed by (insert controlling DoD office) (date of determination) or higher DoD authority.

Distribution Statement F is also used when a document does not contain a distribution statement and no distribution statement can be determined.

☐ **DISTRIBUTION STATEMENT X.** Distribution authorized to U.S. Government Agencies and private individuals or enterprises eligible to obtain export-controlled technical data in accordance with DoDD 5230.25; (date of determination). DoD Controlling Office is (insert controlling DoD office).

Final Report

Application of the Oriented-Eddy Collision Model to Complex Turbulent Flows

Principal Investigator: Blair Perot
Contract Number: N00014-08-1-0275
Dates: 1/1/08 – 12/31/10
Program Officer: Ronald Joslin

Graduate Students: Michael B Martell Jr

Summary

The Oriented-Eddy Collision (OEC) turbulence model hypothesizes that turbulent flow can be modeled as a collection of interacting fluid particles (or eddies) which have fluctuations and an inherent orientation. The model has been formulated in the form of a set of partial differential equations. Underlying this approach is a unique PDF collision model that includes the effect of orientation information along with the usual position and velocity information in the formulation of the probability density function. This adds important physics to the model and differentiates it from most other PDF models and Reynolds-Averaged Navier-Stokes models.

The Oriented Eddy Collision model exactly captures rapid distortion, which is a major shortcoming of most prior Reynolds stress transport models. The ability to predict highly non-equilibrium flow situations well is a major feature of the model. The model automatically (via its construction) satisfies realizability and other known mathematical constraints. It is readily extensible to complex geometries and additional physical affects (such as compressibility, particles, etc). The model has been implemented in the open source CFD framework OpenFOAM for rapid dissemination. It has been tested extensively on basic turbulent flow benchmarks and, more recently, on flows with solid boundaries.

Background

The traditional approach to modeling turbulence (or other types of non-Newtonian fluids) is to hypothesize equations for the unknown stress tensor. Iin turbulence this is the Reynolds stress tensor. Due to the fact that the eddies which make up the flow are roughly the same size as the gradients in the mean flow these eddies respond on similar timescales as the mean flow. This means that algebraic models are rarely predictive, and time-dependent evolution equations for the stress tensor must be hypothesized. In turbulence, these evolution equations are the exact

but unclosed Reynolds stress transport (RST) equations. Simpler turbulence models, such as the $k-\varepsilon$ model or algebraic Reynolds stress models are simplifications of the RST equations.

There is a strong analogy between turbulent fluid flow and non-Newtonian or granular flows. Very similar to turbulent flows, transport equations are very often developed for non-Newtonian stress tensors (the Oldroyd-B model and FENE-P models (Herrechen, *et al.* 1997) are examples). In fact, we note that many important turbulence modeling concepts (realizability, material frame indifference, tensor consistency) actually find their origins in the non-Newtonian literature at this transport equation level. This work is predicated on treating turbulence modeling in a fashion that is similar to non-Newtonian fluid modeling.

It has long been recognized in the non-Newtonian fluid community that transport equation models have serious limitations. An alternative approach is to model the fluid at the particle collision level rather than using a transport equation for the stress. This approach is more versatile, and in many ways, more fundamental. For example, modeling a gas as particles with binary elastic hard sphere collisions gives the Navier-Stokes equations and the perfect gas law when the density is high, but also the correct gas behavior even when the density is low (when Navier-Stokes is not valid). In this work, we investigated the possibility of modeling turbulence as a collection of interacting oriented particles (which will turn out to be disks or rods).

Once a certain collision behavior has been hypothesized there are three very different ways to solve the particle system numerically and obtain a prediction of the fluid behavior. The most straightforward technique is the 'molecular dynamics' approach where one numerically tracks all the particles in the domain, and performs collisions when they occur. This approach has a computational cost equivalent to large eddy simulation (LES) and is not considered further. The other two approaches note that one does not really care what happens to individual particles but only what happens to particles on average. The quantity of interest then becomes the probability density function that describes the probability that a particle (at a certain place and time) has a certain velocity. The evolution of the probability distribution function, *f*, obeys the exact equation

$$\frac{\partial f}{\partial t}+v_i\frac{\partial f}{\partial x_i}+a_i\frac{\partial f}{\partial v_i}+\frac{dn_i}{dt}\frac{\partial f}{\partial n_i}=\left.\frac{df}{dt}\right|_{collisions} \tag{1}$$

where a_i is the acceleration due to external forces (like gravity), n_i is the particle orientation, and the right-hand side describes the average affect of the collisions on the PDF. It is this average collision behavior that we now wish the model to predict. This collision term is also what gives the ensuing model its name. Our collision models assume the collision term has a Fokker-Planck form (see Equations (2) through (4)).

There are three different ways to solve this PDF equation. Using the equivalence between the Fokker-Planck equation and the Langevin equation

(Brownian motion), it is possible to construct a Lagrangian particle method. This is essentially the approach extensively researched by Pope (1994, 2000) and coworkers (with the major difference from this work being that that Pope and others typically do not use oriented eddies, just colliding spheres). In this particle approach, the Lagrangian particles move like Brownian dust particles. They move with the mean flow and are randomly perturbed using a prescription given by the model. In this way each particle is independent from all the others, and simply interacts with the average of all the other particles (*i.e.* the mean flow, and average turbulence statistics). This Monte-Carlo approach is less expensive than tracking and implementing individual collisions ('molecular dynamics' approach) but is still expensive because a large statistical sample of particles that is required. These methods significantly over-resolve the shape compared to what is necessary to model the turbulence.

Using a mesh based method (rather than Monte-Carlo sampling) is also possible. A mesh based method can use a very coarse mesh, thereby lowering the costs involved. A very coarse mesh in velocity space is an idea borrowed from Lattice-Boltzmann numerical methods for solving the Navier-Stokes equations. These methods solve a PDF equation with a very simple collision term that is intended to give Navier-Stokes (Newtonian) fluid behavior. The difference in this work is that we solve a PDF equation with a much more complex collision term (Fokker-Plank), which results in RANS behavior for the fluid (rather than Newtonian). The coarse mesh is acceptable in both cases because the interest is not in the PDF itself but in its lowest order moments - the mean flow and the stresses. These low-order moments can be reasonably extracted from a very coarse approximation of the PDF.

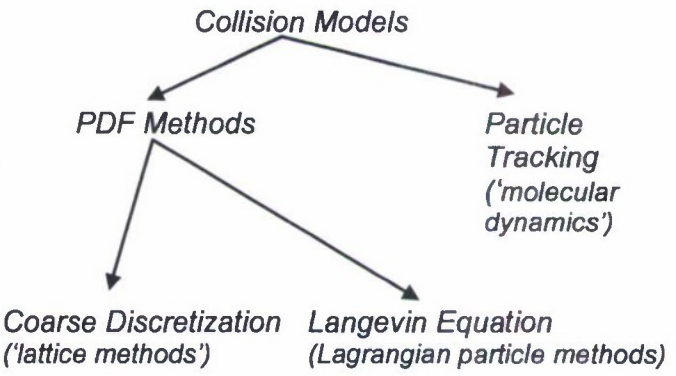

Figure 1: Taxonomy of classic collision model approaches.

Note that the Langevin approach is equivalent to approximating the PDF with a random sample, and a large sample is needed even to approximate the low order moments reasonably well. The Langevin approach is slower because it provides more information (about the higher order moments). Unfortunately, one has little interest, in engineering turbulence models, in the extra information the Langevin solution method provides. These first two approaches to solving the collision model (and the brute force LES-type approach of tracking actual eddies), is shown in Figure 1.

While the coarse mesh approach is inspired by the success of lattice-Boltzmann numerical methods, the approach must be numerically different. This is because the PDF governing molecular interactions (Lattice-Boltzmann) has a variance (width) that is much larger than the mean and which is essentially constant (related to the speed of sound). In contrast, the PDF for turbulence has a variance which is much smaller than

the mean (turbulence intensities are measured in percent), and which can vary significantly (in time or space). This is illustrated in Figure 2:

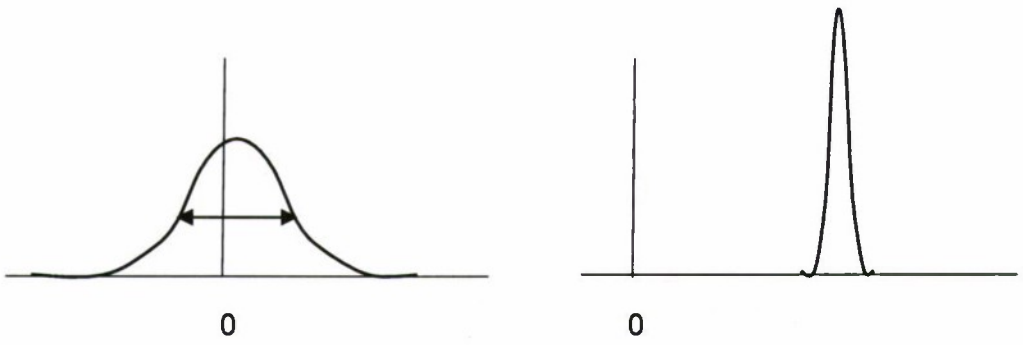

Figure 2: Left - a typical PDF for molecules. Right - A typical PDF for turbulence.

To capture the turbulence PDF with only three points it is necessary to have a moving adaptive mesh in velocity space. In order to avoid losses due to interpolating one mesh to another as the mesh moves, we implemented a fully conservative scheme in which the mesh moves continuously in time (during the time step). This uses technology previously developed by Perot & Nallapati (2003) for moving meshes in physical space. In actual practice the PDF is three-dimensional. An isosurface of an actual PDF (the 50% value) is shown below. This PDF is modeling the behavior of the Le Penven et al (1985) return-to-isotropy Case III > 0 experiment. Note the fairly large changes in the shape and size of the distribution even for this simple experiment. It can also be seen in this figure that a spherical PDF corresponds to isotropic turbulence.

Figure 3: Evolution of the 50% isosurface of the PDF for the return-to-isotropy experiment of Le Penven, *et al.*

The coarse mesh approach was used in our initial ONR work, but the current model actually uses a third PDF equation solution approach that ends up being far more familiar to the CFD users. In the current project we took moments of the PDF collision equation over velocity space in order to construct a set of partial differential

equations for the behavior of each type of oriented disk. No velocity space meshing (or Monte-Carlo sampling) is now necessary. This third approach can be directly included into PDE code frameworks (such as OpenFoam). It has the disadvantage that the third-order correlations must now be modeled (in the pure PDF solutions they can be deduced from the PDF). This means the turbulent diffusion processes must now be modeled.

Theoretical background for the un-orientated eddy collision (EC) model

Lundgren (1967) first derived the exact expression for the collision term in the PDF evolution equation for turbulence. As might be expected, this collision term cannot be expressed solely in terms of the PDF, and solution of the PDF evolution equation therefore requires a model for the collision term. Original development of the OEC model focused on generalizations of the Fokker-Plank collision model (that was derived to describe Brownian motion). In its simplest form this collision model has the form,

$$\left.\frac{df}{dt}\right|_{collision} = -\frac{\partial}{\partial v_i}\left[a\left(v_i - u_i\right)f\right] + b\frac{\partial^2 f}{\partial v_i^{\,2}} \tag{2}$$

where $u_i = \int v_i f dv$ is the mean velocity and a and b are model constants. For turbulence this needs to be generalized. Pope and coworkers (Pope 2000, Reynolds 1995, Van Slooten 1996) use the form,

$$\left.\frac{df}{dt}\right|_{collision} = -\frac{\partial}{\partial v_i}\left[G_{ij}v'_j f\right] + b\frac{\partial^2 f}{\partial v_i^{\,2}} + \nu\frac{\partial^2 f}{\partial x_i^{\,2}} \tag{3}$$

where $v'_j = v_j - u_j$ is the fluctuating velocity and the first term (the drift term) now has a matrix model parameter G_{ij}, and a viscous term has been added for near wall (low Re number) calculations. The conversion of these Fokker-Planck models to a Langevin equation for numerical solution dictates that the diffusion term (with *b*) be isotropic and not have a tensor coefficient.

Original development of the OEC model analyzed the following even more generalized Fokker Plank model.

$$\begin{aligned}\left.\frac{df}{dt}\right|_{collision} = &-\frac{\partial}{\partial v_i}\left[G_{ij}v'_j f\right] + \frac{\partial}{\partial v_i}\left[H_{ij}\frac{\partial f}{\partial v_j}\right] + \frac{\partial}{\partial v_i}\left[\left(J_{ij} + \nu u_{i,j}\right)\frac{\partial f}{\partial x_j}\right] \\ &+ \frac{\partial}{\partial x_i}\left[\nu\frac{\partial f}{\partial x_i}\right] + \frac{\partial}{\partial v_i}\left[\nu K_{,n}\frac{\partial\left(fv'_i/K\right)}{\partial x_n}\right] + \left.\frac{dv_i}{dt}\right|_{mesh}\frac{\partial f}{\partial v_i}\end{aligned} \tag{4}$$

The last term on the right hand side accounts (exactly) for the coarse mesh motion in velocity space (to track the PDF). The first three terms involve model tensors. Sometimes, these tensors are isotropic and governed by a single parameter. The viscous terms account for low Reynolds number effects and strong inhomogeneity. They do not involve any additional parameters and were derived via analysis and the condition that the model be exact as it approaches a wall (in the laminar sub layer).

The zeroth moment of the PDF equation (Equation (4)) is the mass conservation equation. The first velocity moment of the PDF equation gives the momentum equation,

$$\frac{\partial u_n}{\partial t}+\frac{\partial(u_i u_n+R_{in})}{\partial x_i}-a_n=\frac{\partial}{\partial x_i}\left[\nu u_{n,i}\right] \tag{5}$$

This implies that the acceleration is given by $a_n=-p_{,n}+(\mu u_{i,n})_{,i}$. The viscous contribution to this acceleration is necessary only if the viscosity is not constant. Taking the moment of the modeled PDF equation with respect to $v'_n v'_m$ gives the Reynolds stress transport equation,

$$\begin{aligned}\frac{\partial R_{nm}}{\partial t}+\frac{\partial(u_i R_{nm})}{\partial x_i}+\frac{\partial T_{nmi}}{\partial x_i}+(u_{m,j}R_{jn}+u_{n,j}R_{jm})=(G_{mj}R_{jn}+G_{nj}R_{jm})+(H_{nm}+H_{mn})\\ -(J_{mj}u_{n,j}+J_{nj}u_{m,j})+\frac{\partial}{\partial x_i}\left[\nu\frac{\partial R_{jm}}{\partial x_i}\right]-2\nu K_{,j}\frac{\partial\left(R_{mn}/K\right)}{\partial x_j}\end{aligned} \tag{6}$$

where $T_{nmi}=\int v'_n v'_m v'_i f d\mathbf{v}$ and $K=\frac{1}{2}R_{ii}$ is the turbulent kinetic energy. The tensors G_{ij}, H_{ij}, and J_{ij} determine the model. Complex dissipation and pressure-strain models can be implemented via these tensors.

The equation for the total resolved (or mean) kinetic energy, $E_r=\int\frac{1}{2}v_i v_i f d\mathbf{v}-\frac{1}{2}R_{ii}$, is

$$\frac{\partial E_r}{\partial t}+\frac{\partial}{\partial x_i}\left[u_i E_r+u_k(R_{ik}-\nu u_{i,k})\right]=-(pu_i)_{,i}+u_{n,j}R_{jn}-\nu u_{i,j}(u_{i,j}+u_{j,i})+\frac{\partial}{\partial x_i}\left[\nu\frac{\partial E_r}{\partial x_i}\right] \tag{7}$$

The resolved kinetic energy correctly loses energy as a result of large scale dissipation, and via turbulence production. It is completely specified and does not depend on the model coefficients. The details of these derivations can be found in Chartrand (2005).

When implementing the Fokker-Planck collision model (Eqn. 4) on a coarse mesh, it is attractive to make the change of variables $\hat{f}=\ln(f)$. If *f* is close to

Gaussian (which is expected) then $\hat{f}$ will be close to parabolic. This parabola can be accurately resolved and interpolated by the three points available in our scheme. The evolution equation for $\hat{f}$ is,

$$\frac{\partial \hat{f}}{\partial t}+v_i\frac{\partial \hat{f}}{\partial x_i}+(a_i-a_{mesh})\frac{\partial \hat{f}}{\partial v_i}=-\dot{G_{ii}}-G_{ij}v_j'\frac{\partial \hat{f}}{\partial v_i}+\frac{\partial}{\partial v_i}\left[H_{ij}\frac{\partial \hat{f}}{\partial v_j}\right]+H_{ij}\frac{\partial \hat{f}}{\partial v_i}\frac{\partial \hat{f}}{\partial v_j}$$
$$+\frac{\partial}{\partial v_i}\left[(J_{ij}+\nu u_{i,j})\frac{\partial \hat{f}}{\partial x_j}\right]+(J_{ij}+\nu u_{i,j})\frac{\partial \hat{f}}{\partial x_j}\frac{\partial \hat{f}}{\partial v_i}+\frac{\partial}{\partial x_i}\left[\nu\frac{\partial \hat{f}}{\partial x_i}\right]+\nu\frac{\partial \hat{f}}{\partial x_i}\frac{\partial \hat{f}}{\partial x_i} \quad (8)$$
$$+\nu K_{,n}\left[\frac{\partial}{\partial x_n}+\frac{\partial \hat{f}}{\partial x_n}\right]\left\{\frac{3}{K}+\frac{v_i'}{K}\frac{\partial \hat{f}}{\partial v_i}\right\}$$

While there are more terms to compute in this version, the equation for $\hat{f}$ is much more accurate to solve numerically. In addition, low order methods and simple (3 point) difference stencils suffice because $\hat{f}$ is expected to be very close to quadratic.

The models for the tensors G_{ij}, H_{ij}, and J_{ij} require a time scale to be dimensionally correct. For this reason an additional transport equation for the timescale must be included in the model. The un-oriented eddy model therefore used the standard epsilon transport equation for this purpose since it is very commonly used in RST models as well. The oriented model obtains the timescale from the orientation vector whose length represents the inverse of the eddy size. So no scale equation is necessary in the most recent model implementation.

The Original Model

The original collision model first proposed by Perot and Chartrand (2005) was

$$G_{ij}=C_{p2}^{s}S_{ij}+C_{p2}^{w}\overline{W}_{ij}+\tfrac{1}{2}C_{p2}^{s}\frac{P}{K}\delta_{ij}-\frac{\hat{\varepsilon}}{R_{nm}R_{mn}}R_{ij}-\frac{\hat{\varepsilon}}{K}C_d\delta_{ij} \quad (9)$$

$$H_{ij}=\tfrac{\hat{\varepsilon}}{K}C_dR_{ij} \quad (10)$$

$$J_{ij}=-\tfrac{2}{3}KC_{p2}^{*}\delta_{ij} \quad (11)$$

where $\hat{\varepsilon}=\varepsilon\left(1+10\nu\left|\left(\sqrt{K}\right)_{,i}\right|/K\right)^{-1}$ is the modified dissipation that goes to zero in regions of strong inhomogeneity such as near walls, and $P=-R_{nm}u_{n,m}$ is the standard turbulent production rate. The frame invariant strain-rate and rotation-rate tensors are

respectively $S_{ij} = \frac{1}{2}(u_{i,j} + u_{j,i})$ and $\overline{W}_{ij} = \frac{1}{2}(u_{i,j} - u_{j,i}) + \varepsilon_{ijk}\Omega_k$, where Ω_k is the rotation rate of a non-inertial frame of reference.

For comparison with classic RST models, the equivalent Reynolds stress transport equation would be,

$$\begin{aligned}
&\frac{\partial R_{mn}}{\partial t} + \frac{\partial}{\partial x_i} u_i R_{mn} + \frac{\partial}{\partial x_i} T_{imn} + \left(u_{m,j} R_{jn} + u_{n,j} R_{jm}\right) = \\
&\quad \left(C^s_{p2} S_{mj} + C^w_{p2} W_{mj}\right) R_{jn} + \left(C^s_{p2} S_{nj} + C^w_{p2} W_{nj}\right) R_{jm} \\
&\quad + C^s_{p2} \frac{P}{K} R_{mn} - 2\frac{\hat{\varepsilon}}{R_{ij} R_{ji}} R_{ms} R_{sn} \\
&\quad + \tfrac{4}{3} K C^*_{p2} S_{mn} + \frac{\partial}{\partial x_i} \nu \frac{\partial R_{mn}}{\partial x_i} - 2\nu \frac{\partial K}{\partial x_l}\left(\frac{R_{mn}}{K}\right)_{,l}
\end{aligned} \tag{12}$$

Note that the model constant C_d does not affect the Reynolds stress transport equation. However, it does have an effect on the higher order moments (such as T_{imn}) and the turbulent transport term. This constant can be related to the Kolmorgorov constant (Pope 2000). The other model constants are actually parameters and are given by,

$$C^s_{p2} = \frac{\nu_t}{\nu + \nu_t} - .2F, \qquad C^w_{p2} = \frac{\nu_t}{\nu + \nu_t} - .4F, \qquad C^*_{p2} = -0.2F^2 + .006\frac{P}{\hat{\varepsilon}} \tag{13}$$

where the eddy viscosity is given by $\nu_t = .12F\frac{K^2}{\hat{\varepsilon}}$ and $F = \frac{27}{8}\det(R_{ij}/k)$ is the standard two-component parameter that is unity in isotropic turbulence and zero for two-component turbulence.

The transport model for the epsilon equation is standard and is given by

$$\frac{\partial \varepsilon}{\partial t} + u_i \frac{\partial \varepsilon}{\partial x_i} = \frac{\hat{\varepsilon}}{K}(C_{\varepsilon 1} P - C_{\varepsilon 2}\varepsilon) + \frac{\partial}{\partial x_i}(\nu + C_{\varepsilon 3}\nu_T)\frac{\partial \varepsilon}{\partial x_i} \tag{14}$$

where $C_{\varepsilon 1} = 1.43$, $C_{\varepsilon 2} = 11/6$, $C_{\varepsilon 3} = 0.83$, and fairly standard values.

Inspiration for OEC

The analysis above lays the groundwork for the oriented eddy collision model. A brief review of PDF-based models is in order.

Boltzmann and Fokker-Planck

It is helpful to begin with a simple case, and not consider complications such as colliding oriented eddies. Instead, consider a collection of particles: an expression can be found for the number of particles that have some velocity v_i at location x_i and time t, called a number density function. The more familiar probability density function is simply the number density divided by the total number of particles under consideration. Let $f(v_i, x_i, t)$ be the probability density function. Using this function, one can arrive at several useful quantities: multiplying f by v_i and integrating over all of the possible velocities (that is, taking the first moment of f and integrating over velocity space), one can arrive at the mean velocity for the collection of particles, U_i:

$$U_i = \int_{v_i} v_i f(v_i, x_i, t) dv_i \tag{15}$$

where $\int_{v_i}$ and dv_i imply a triple integral over $v_i, i = 1,2,3$. If the mean velocity can be found, perhaps another quantity of interest, $\overline{u_i u_j}$ can be found. Taking the second moment of f with the fluctuating velocities $v_i - U_i$, recalling the fluctuating velocities are the total velocity of a given particle v_i with the mean velocity of all particles U_i subtracted off:

$$\overline{u_i u_j} = \int_{v_i} (v_i - U_i)(v_j - U_j) f(v_i, x_i, t) dv_i \tag{16}$$

once again recognizing that a triple integral exists in Equation (15). Equations (15) and (16) represent the statistical mechanics of the collection of particles but say nothing about the physics present in that f has yet to be prescribed. One of the simplest ways to describe the time evolution of a PDF is through the Boltzmann equation, which essentially models particle collisions by relaxing their PDFs to the mean:

$$\frac{\partial}{\partial t} f(v_i, x_i, t) + v_i \frac{\partial}{\partial x_i} f(v_i, x_i, t)$$
$$+ a_i \frac{\partial}{\partial v_i} f(v_i, x_i, t) = \frac{\partial}{\partial t} f(v_i, x_i, t)\Big|_{collisions} \tag{17}$$

with a_i representing some body (external) force that may be acting on the fluid (such as a Coriolis term) and the right hand side representing the way in which the average of all collisions over time affects the PDF. The left hand side of Equation (17) is exact, while the right hand side is that which requires a model, the so-called ``collision'' term. An approximation to the Boltzmann equation, such as the one originally proposed by Bhatnagar, *et. al* (1954) can be employed and slowly brings f to an equilibrium value, which usually means a Gaussian distribution. Once a form of f has been chosen, it can be used in Equation (15) and the mean velocity found (the method in which this is done will be discussed later). A linear relaxation model may also be employed (see Perot & Chartrand's earlier work). Interestingly, for low density flows (meaning flows in which few particle collisions occur), a simple collision model returns the ideal gas law, the viscous terms of the Navier Stokes equations, Fourier heat conduction and many other physical processes. Thus, this method is suited for Newtonian flows, but might not work well as a turbulence model. Inspecting the second moment and plugging the Boltzmann equation in to Equation (16) yields an unfortunate result: this simple collision model predicts that the Reynolds stresses are zero, $\partial \overline{u_i u_j} / \partial t = 0$. Not only is this approach flawed, it is in fact useless for capturing the behavior of a turbulent flow. This is due to the fact that the Boltzmann equations look at fluid interactions purely as a viscous phenomenon with a single relevant time scale, an idea which sounds familiar from previous turbulence models considered. It was already determined that this assumption will never capture turbulence properly, and it is no surprise that this method fails.

An alternative to the Boltzmann equation is the Fokker-Planck (FP) equation (also referred to as the Kolmogorov forward equation from Kolmogorov (1942)), which describes the time evolution of a PDF in a more complicated way:

$$\frac{\partial}{\partial t} f(v_i, x_i, t) + v_i \frac{\partial}{\partial x_i} f(v_i, x_i, t) + a_i \frac{\partial}{\partial v_i} f(v_i, x_i, t)$$
$$= -\alpha \frac{\partial}{\partial v_i}(v_i - U_i) f(v_i, v_i, t) + \beta \frac{\partial^2}{\partial v_i^2} f(v_i, x_i, t) \tag{18}$$

with α and β model constants. Equation (18) (adapted from Perot & Chartrand 2005) represents one of the simplest Fokker-Planck collision models with the right hand side of Equation (17) replaced by two terms. The right hand side of Equation (18) must be

generalized in order to be employed for PDF turbulence model methods. Pope and others proposed a generalized form, and use it extensively in their PDF method work (see Pope 2000, Pope 1982, Pope 1983, Perot & Chartrand 2005 and more):

$$\frac{\partial}{\partial \mathrm{t}} f(v_i, x_i, t) + v_i \frac{\partial}{\partial x_i} f(v_i, x_i, t) + a_i \frac{\partial}{\partial v_i} f(v_i, x_i, t)$$
$$= -\frac{\partial}{\partial v_j}\left[G_{ij}(v_i - U_i) f(v_i, x_i, t) \right] + \beta \frac{\partial^2}{\partial v_i^2} f(v_i, x_i, t) + \nu \frac{\partial^2}{\partial x_i^2} f(v_i, x_i, t) \quad (19)$$

where G_{ij} is a tensorial modeling parameter, ν the fluid viscosity, and noting the addition of a second order spatial derivative (Laplacian) of the PDF. Unlike the Boltzmann equation, the FP approach captures more than just viscous Navier-Stokes, and the second moment is not zero.

The two methods mentioned above relate to the aforementioned Langevin equation: a Langevin approach can be employed to solve the resulting PDF transport equations arrived at from plugging either the Boltzmann or the Fokker-Planck collision models in to Equation (17) and the resulting expression for f in to Equations (15) or (16). This is because the equations may be solved using ``normal'' methods, that is using a finite-difference or finite-element method or may be solved by using a particle approach, the details of which will be avoided here. Using a Langevin approach makes no changes to the underlying physics - it is simply a particle method solution. When a Langevin method is used with a Boltzmann equation, this is often referred to as a Lattice-Boltzmann method (as the Boltzmann equation is solved in a lattice of points, dictated by the Langevin equation). Solving a PDF collision method in this way is akin to solving Navier Stokes without turbulent terms. Solving the Fokker-Planck model using a Langevin method results in a means of solving the Reynolds-averaged Navier Stokes equations in the form of a Reynolds stress transport model. This method is referred to by Pope as the Generalized Langevin Method (GLM) (Pope 2000, Pope 1994, Haworth 1985). Various forms of the Fokker-Planck model lead to various forms of Reynolds stress transport models, ranging from the simpler Launder, Reece, and Rodi (Launder, *et al.* 1974) to more complex forms. The fact that well-known turbulence models emerge from the steps above could be considered affirmation that the analysis was correct. However, simply returning to a statistical mechanics-based version of a well known turbulence model family also means that the new PDF method inherits many of the previous problems associated with RST models, most important of which is the inability to capture linear (rapid distortion theory limit) turbulence. Despite the fact that PDF methods require no model for the triple correlation $\overline{u_k u_i u_j}$ (assuming they remain in PDF and not RST form), they still suffer from many problems. This calls in to question the need to accurately model the triple correlation and suggests that perhaps it is in the pressure term that the missing physics may be found.

Advanced methods

Taking a step back from PDF methods for a moment, the recent work of Reynolds & Kassinos (1996) will be considered briefly. Reynolds & Kassinos wished to capture rapidly deforming homogenous turbulence with a Reynolds stress transport model. They hypothesized that the stress tensor was not enough to capture rapid distortion theory limit turbulence as information about the turbulent structure was not contained within such a quantity. Among others, they proposed a general model which transports a single, rank two tensor, the "eddy axis tensor" which characterizes the shape and orientation of a turbulent eddy. The model employed algebraic equations of state (as opposed to a stress tensor) and two scalar quantities thus containing information about the dimensionality and "componentality" of the turbulence (Reynolds & Kassinos 1996). The model managed to capture many linear turbulence cases exactly, which was the first ever demonstration of an RST-like turbulence model providing accurate solutions in this limit of turbulence. Unfortunately, many considered the model difficult to understand (this author included) mainly due to the fact that the entire model was formed in wave (Fourier) space. Despite this issue, the work produced a powerful idea: Perhaps the failure of PDF-based turbulence models lie not in the formation of the PDF collision model (*e.g.* Fokker-Planck) but instead in a previously unimagined missing unknown, perhaps related to orientation of turbulent eddies or, in the case of PDF methods, fluid particles.

Perot & Chartrand (2005) proposed a very general Fokker-Planck collision model with more unknowns than the general Fokker-Planck model proposed by Pope (2000):

$$\frac{\partial f}{\partial t}+v_i\frac{\partial f}{\partial x_i}+a_i\frac{\partial f}{\partial v_i}=-\frac{\partial}{\partial v_j}\left[G_{ij}(v_i-U_i)P\right]+\frac{\partial}{\partial v_j}\left[H_{ij}\frac{\partial f}{\partial v_j}\right]$$
$$+\frac{\partial}{\partial v_j}\left[(J_{ij}+\nu u_{i,j}\frac{\partial f}{\partial x_j}\right]+\frac{\partial}{\partial x_i}\left[\nu\frac{\partial f}{\partial x_i}\right]+\frac{\partial}{\partial v_i}\left[\nu K_{,n}\frac{\partial}{\partial x_n}\left(\frac{Pv_i}{K}\right)\right] \quad (20)$$

with an additional term added to the end of Equation (20) to account for mesh motion, which was related to a numerical method used by Perot & Chartrand to solve their generalized Fokker-Planck method using an adaptive three-point mesh in velocity space (Perot & Chartrand 2005). In Equation (20), G_{ij}, H_{ij} and J_{ij} are tensorial modeling terms, $u_{i,j}$ is the physical-space velocity gradient and $K_{,n}$ the physical-space gradient of the kinetic energy. Van Slooten and Pope (1996), and more recently Perot and coworkers have attempted to overcome the inherent limitations of Fokker-Planck based PDF turbulence models. Work by Perot determined that any extension of the Fokker-Planck model would simply result in a slightly more complex but still inherently limited RST model, unless orientation was given to the fluid particles, that is a Fokker-Planck collision model was formed for something like rods or disks (later called eddies) rather than particles which are spheres and have no orientation. This can be achieved

by adding an ``extra'' unknown to a Fokker-Planck like collision model yielding derivatives with respect to time, space, and the extra term, which could be thought of as eddy orientation.

Van Slooten and Pope (1996) furthered the ideas presented by Reynolds & Kassinos (1995) first by applying them to a PDF-based method solved with a particle-based approach (a Monte-Carlo solution), and then using this new method to simulate *inhomogeneous* linear turbulence. They implemented this extra information via a joint PDF of velocity and a ``wave vector'' which is related to the unit wave vector tied to a given turbulent eddy size. The collection of these vectors are referred to as the directional spectrum. This was a major step forward in PDF-based turbulence modeling, but the method is both difficult to understand and expensive to solve, requiring a large statistical sample in order to return reasonable results from the particle-based solution. Furthermore, Van Slooten & Pope point out the need for improved dissipation models.

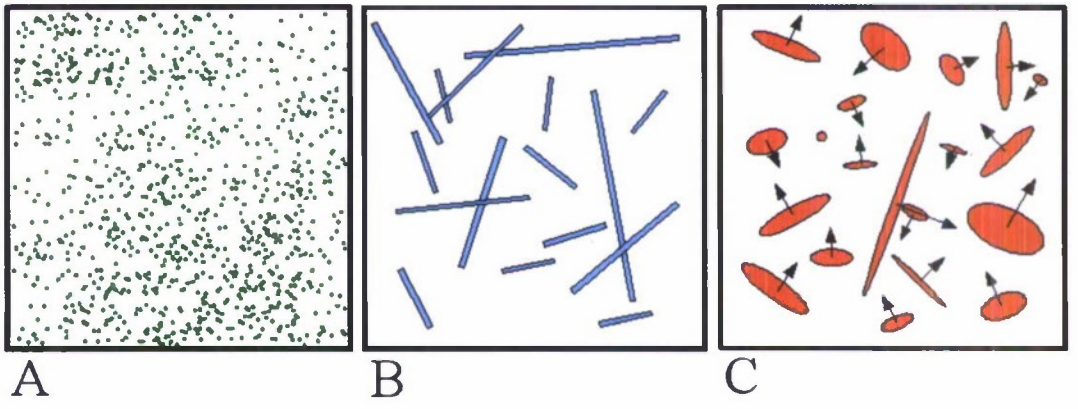

Figure 4: Box A illustrates a hypothetical region of turbulent fluid as a classic particle collision model, like Fokker-Planck or Boltzmann. The particles are spheres and cannot have any orientation. Box B is a schematic of the same flow but with an expanded collision model that treats particles as rods rather than spheres, thus including orientation information. Finally, box C illustrates disks (eddies), which appear to be the shape necessary in order to capture linear turbulence.

Perot and Chartrand picked up where Van Slooten and Pope left off, believing that the key to linear turbulence was indeed the extra ``information'' contained within the wave vectors. They chose to add this information as a second derivative to the generalized Fokker-Planck Equation (17):

$$\frac{\partial}{\partial t} f + v_i \frac{\partial}{\partial x_i} f + a_i \frac{\partial}{\partial v_i} f = -\frac{\partial}{\partial v_j}\left[G_{ij}(v_i - U_i) f \right] + \frac{\partial^2}{\partial q_j^2}\left[H_{ij} q_i f \right] + \beta \frac{\partial^2}{\partial v_i^2} f + \nu \frac{\partial^2}{\partial x_i^2} f \qquad (21)$$

noting the second derivative in *orientation space*, here denoted by the unknown vector q_i. This term acts as a sort of advection in orientation space, and ends up being responsible for the decay terms present in the RST equation form of the eddy orientation vector evolution equation. Perot and Chartrand interpreted this extra information as eddy orientation (similar to Reynolds' and Kassinos' hypothesis), but chose to transform the PDF collision model in to a RST equation form. The resulting model was like a classic RST model but had extra information inherent to it, resulting in a model which could capture fast pressure strain exactly, yielded excellent experimental agreement in elliptical flows, and calculated linear turbulence exactly. The dissipation term still required model tuning, but nearly all RST model issues had been resolved. Furthermore, unlike the PDF form, when cast as an RST model the turbulent transport term required a model, but models for this term are abundant and not difficult to form. Figure 4 is a schematic illustration of this concept. A critical difference exists between the model proposed by Reynolds & Kassinos (1996) and that of Perot: Perot's real-space eddy orientation model did not take the moment of and subsequently integrate over orientation space, whereas Reynolds & Kassinos did. This step allowed Reynolds & Kassinos to cast their model in the form of a Reynolds stress transport model which, in order to then incorporate the extra unknown, they multiplied with the unknown vector yielding a *third* rank tensor transport equation. By choosing to forgo this moment, Perot kept orientation in the Reynolds stress equation itself. This enabled the evolution of the orientations to be prescribed in such as way that the full Reynolds stress transport equation, complete with included orientation information, was exact in the limit of linear turbulence.

More recent work by Perot, Chartrand and Andeme (2008) furthered progress on the Oriented Eddy collision model, treating it, for the most part, as a modified RST model rather than a PDF collision model. As was previously mentioned, Perot & Chartrand chose not to integrate over orientation space thus one Reynolds stress equation exists for each eddy orientation vector, and the average (that is, RANS-like) Reynolds stress tensor is a simple average of all of the individual, per-eddy Reynolds stress tensors. Perot and Chartrand proposed the followings per-eddy Reynolds stress evolution equation (note that nomenclature has been updated from Chartrand (2005) to be consistent with current versions of the model):

$$R_{ij,t} + \nabla\left(\overline{u}_k R_{ij}\right) = \tag{22}$$

$$\left[\overline{u}_{i,k} + \left(\frac{q_i q_l}{q^2} - \delta_{il}\right) 2\overline{u}^*_{l,k}\right] R_{kj} + \left[\overline{u}_{j,k} + \left(\frac{q_j q_l}{q^2} - \delta_{jl}\right) 2\overline{u}^*_{l,k}\right] R_{ki} \tag{23}$$

$$-\left(\alpha \nu \overline{q^2} + \frac{1}{\tau_R}\right) R_{ij} \tag{24}$$

$$-\frac{C_1}{\tau_R}\left(\frac{1}{1+C_2\dfrac{\nu}{\nu_T}}\right)\left[R_{ij}-\bar{K}\left(\delta_{ij}-\frac{q_i q_j}{q^2}\right)\right] \tag{25}$$

$$+\left(R_{lj}\frac{q_i}{q^2}+R_{li}\frac{q_j}{q^2}\right)\left(A_l+B_l\right) \tag{26}$$

$$+\left[\left(\nu+\nu_T\right)R_{ij,k}\right]_{,k} \tag{27}$$

with R_{ij} the Reynolds stress tensor (one for each eddy), q_i the eddy orientation vector (and the quantity that makes this model look unusual compared with a classic RST model), turbulent viscosity $\nu_T=\sqrt{\overline{K^2}/\overline{Kq^2}}$ noting an over bar indicates the quantity averaged over all eddies, time scale $1/\tau_R=\sqrt{\bar{K}\overline{q^2}}$, Kronecker delta δ_{ij}, average velocity $\bar{u}_i$, and constants C_1, C_2 and α. Note that model also includes information about the rotation vector for a non-inertial frame Ω_k in $\bar{u}^{\bullet}_{i,k}$, namely $\bar{u}^{\bullet}_{i,k}=\bar{u}_{i,k}+\epsilon_{ikj}\Omega_k$, with ϵ_{ikj} being the permutation tensor. Equation (22) is the material derivative of the Reynolds stress tensor. Equation (23) handles the stress tensor production, while Equation (24) accounts for viscous dissipation. Equation (25) provides a return-to-isotropy model for the Reynolds stresses (Perot & de Bruyn Kops 2006), and Equation (26) ensures that the Reynolds stress tensor and eddy orientation vector (q_i) remain orthogonal, which is akin to enforcing incompressibility (Chartrand 2005). The terms A_l+B_l represent the return-to-isotropy model for the eddy vectors and a system rotation term, respectively. Equation (27) is of course the viscous diffusion. It is instructive to examine the eddy orientation evolution equation before these other quantities are described:

$$q_{i,t}+\nabla\cdot\left(\bar{u}_j q_i\right)= \tag{28}$$

$$-q_k\bar{u}_{k,i} \tag{29}$$

$$-\frac{1}{3}\left(\alpha\nu\overline{q^2}+\frac{1}{\tau_R}\right)q_i \tag{30}$$

$$-\left(A_i+B_i\right) \tag{31}$$

$$+\frac{1}{3}\left[\left(\nu+\nu_T\right)q_{i,k}\right]_{,k} \tag{32}$$

where Equation (28) is the material derivative of the eddy orientation vector, Equation (29) handles production with Equation (30) providing for dissipation and Equation (31)

being the standard diffusion term. Equation (31) has the eddy vector return-to-isotropy term A_i and rotation term B_i.

$$A_i = \frac{C_3}{\tau_R}\left(\frac{1}{1+C_2\dfrac{\nu}{\nu_T}}\right)\left[3N_{ki}-\delta_{ki}\right]q_k \tag{33}$$

with constant C_3 and $N_{ki}=\overline{q_i q_k}/\overline{q^2}$. The rotation term B_i ensures that the model responds properly to rotation of non-inertial frame, and is defined as

$$B_i = \frac{1}{\tau_R}\left[\frac{\overline{\left(q_k/\Omega_k^*\right)^2/q^2}}{20\overline{q^2}\,\overline{K}+0.25\left(\Omega_k^*\right)^2}\right]q_i \tag{34}$$

with the vorticity vector defined as $\Omega_k^* = \epsilon_{ijk}\overline{u}_{k,j}+\Omega_i$ recalling Ω_i is the rotation vector for a non-inertial frame.

The origins of the terms above are described in detail by Chartrand (2005) They are explained briefly below. The dissipation terms (Equations (24) and (30)) come from observations of isotropic decay. The part of the parenthetical term $\alpha\nu q^2$ originates from low Reynolds number decay. The second term $1/\tau_R$ handles high Reynolds number decay. These are arguably the simplest terms in the model, and were constructed first. Next, the production terms (Equations (23) & (29)) were constructed using the exact linearized Navier Stokes equations for rapid distortion theory from Pope (2000):

$$\frac{\partial R_{ij}}{\partial t} = \left[\overline{u}_{i,k}+\left(\frac{k_i k_l}{k^2}-\delta_{il}\right)2\overline{u}^*_{l,k}\right]R_{kj}+\left[\overline{u}_{j,k}+\left(\frac{k_j k_l}{k^2}-\delta_{jl}\right)2\overline{u}^*_{l,k}\right]R_{ki} \tag{35}$$

$$\frac{\partial k_i}{\partial t} = -k_k\frac{\partial \overline{u}_k}{\partial x_i} \tag{36}$$

noting that k_i is Pope's wave vector and that this is directly analogous to the eddy orientation vector q_i. The similarities between the exact RDT limit of the Navier Stokes equations and the production terms for R_{ij} and q_i are easy to see. The production and dissipation terms to achieve viscous RDT. Anisotropic decay was tackled next. It is interesting to note that this is first time that inter-eddy interactions must be accounted for. Rotta's linear return to isotropy model (Rotta 1951) for the stress tensor was tested

first. This version varied slightly from Equation (32) in that rather than an average kinetic energy $\overline{K}$ being employed, the local $K = \frac{1}{2} R_{mm}$ was employed. The so-called "global" version was also tested, and found to perform better (Perot & Chartrand 2005). Chartrand and Perot also tested their non-linear "EG" return model and found it deficient in this application, thus choosing the ``global" Rotta-like return to include in OEC. Isotropy in OEC is not only by isotropic Reynolds stresses (on a local, per eddy level) but also uniform distribution of unit eddy orientation vectors on a unit sphere. Flows tend to distort their distribution and a method is needed to return to an isotropic state. Chartrand (2005) investigated six different methods, the details of which will be avoided here. The method employed in Equation (33) calculates the normalized distribution of the eddy vectors N_{ki} and projects the eddy vectors according to the difference between the normalizes distribution and the *isotropic* normalized distribution represented by the Kronecker delta δ_{ki}.

The Complete Original OEC model

The original OEC model evolves two quantities: the eddy orientation vectors, $\hat{q}_i$ and the Reynolds stresses $\hat{R}_{ij}$ with the kinetic energy $\hat{k}$ calculated from the Reynolds stresses as $\hat{k} = \hat{R}_{ii}/2$. The Reynolds stresses are averaged over all eddies to produce R_{ij} which is then used in the momentum equation. The original OEC model was posed as:

$$\frac{\partial \hat{R}_{ij}}{\partial t} + \nabla \cdot \left(\overline{u}_k \hat{R}_{ij} \right) = \hat{P}_{ij} - \left(\alpha \nu \hat{q}^2 + \frac{1}{\tau_R} \right) \hat{R}_{ij} - \hat{R}_{ij}^{\,R} + \hat{M}_{ij} + \nabla \cdot \left(\nu + \hat{\nu}_t \right) \nabla \hat{R}_{ij} \tag{37}$$

$$\frac{\partial \hat{q}_i}{\partial t} + \nabla \cdot \left(\overline{u}_j \hat{q}_i \right) = -\hat{q}_k \overline{u}_{k,i} - \frac{1}{C_p + 1} \left(\alpha \cdot \nu \hat{q}^2 + \frac{1}{\tau_R} \right) \hat{q}_i - (\hat{q}_l^{\,R} + \hat{s}_l) + \nabla (\nu + \hat{\nu}_t) \nabla \hat{q}_i \tag{38}$$

The first equation above evolves the eddy orientation vectors $\hat{q}_i$ while the second handles the local (per-eddy) Reynolds stresses $\hat{R}_{ij}$. Return to isotropy for $\hat{q}_i$ is handled by $\hat{q}_l^{\,R}$, defined as

$$\hat{q}_l^{\,R} = \frac{1}{\tau_R} \left(\frac{C_{qR}^{\,Up}}{1 + C_{qR}^{\,Dn} \left(\frac{\nu}{\nu_T} \right)} \right) \left(3 \frac{\hat{q}_i^{\,2}}{q_i^{\,2}} N_{ki} - \delta_{ki} \right) \hat{q}_k \tag{39}$$

with $N_{ki} = \left[(1/N) \sum \hat{q}_k \hat{q}_i \right] / q_i^{\,2}$ and constants $C_{qR}^{\,Up}$ and $C_{qR}^{\,Dn}$. Note that $C_{qR}^{\,Up}$ has been abandoned in new versions of OEC, discussed below. Return to isotropy for $\hat{R}_{ij}$ is similarly handled by $\hat{R}_{ij}^{\,R}$ defined as

$$\hat{R}_{ij}{}^{R} = \frac{1}{\tau_R}\left(\frac{C_{RR}{}^{Up}}{1+C_{RR}{}^{Dn}\left(\frac{\nu}{\nu_T}\right)}\right)\left[\hat{R}_{ij} - K\left(\delta_{ij} - \frac{\hat{q}_i\hat{q}_j}{\hat{q}^2}\right)\right] \tag{40}$$

with constants $C^{Up}{}_{RR}$ and $C^{Dn}{}_{RR}$. $\hat{M}_{ij}$ combines rotation, eddy vector return to isotropy and a term which ensures $\hat{q}_i$ and $\hat{R}_{ij}$ are orthogonal, as shown in below:

$$\hat{M}_{ij} = \left(\hat{R}_{lj}\frac{\hat{q}_i}{\hat{q}^2} + \hat{R}_{li}\frac{\hat{q}_j}{\hat{q}^2}\right)(\hat{q}_l{}^{R} + \hat{s}_l) \tag{41}$$

It is important to note that several major nomenclature changes have occurred since this form of the model was created. Hats $\hat{}$ now indicate models based on a variant of eddy vector (to be introduced later) and over bars now indicate averages taken over eddies. The eddy vector return term $\hat{q}_l{}^{R}$ is now denoted simply A_i while the system rotation term $\hat{s}_l$ has become B_i. To be consistent, the Reynolds stress return to isotropy term $\hat{R}_{ij}{}^{R}$ is now A_{ij} (to avoid confusing superscripts), the per-eddy local kinetic energy is K and the eddy-averaged (often called global) kinetic energy is simply $\overline{K}$. The same scheme is used for the Reynolds stresses and eddy vectors.

Validation

Previous work on the oriented eddy collision model has resulted in the model being validated across a wide variety of cases, both simple and complex turbulent flows. Considering OEC's implementation in OpenFOAM, numerous validation cases were re-run. Furthermore, several major modifications have been made to the basic model including the addition of terms to handle near-wall asymptotic behavior of the eddy vector and Reynolds stress tensor, the inclusion of a near-wall eddy rotation term in an attempt to capture non-local wall effects (discussed later), the removal of several modeling constants, and the derivation of three additional forms of the OEC model whose aim it is to increase the numerical, temporal, and near-wall stability of the model. Considering these changes, and the necessity to recreate many benchmark cases in a manner useable by OpenFOAM, many previously performed tests were once again performed, including one of the simplest cases, isotropic, homogenous decay:

Table 1: Initial conditions from de Bruyn Kops' DNS of isotropic homogeneous decay

de Bruyn Kops (DNS)	
$\varepsilon(m^2/s^3)$	0.782
$K(m^2/s^2)$	0.087
$v(m^2/s)$	1.49e- 5
Re_T	655

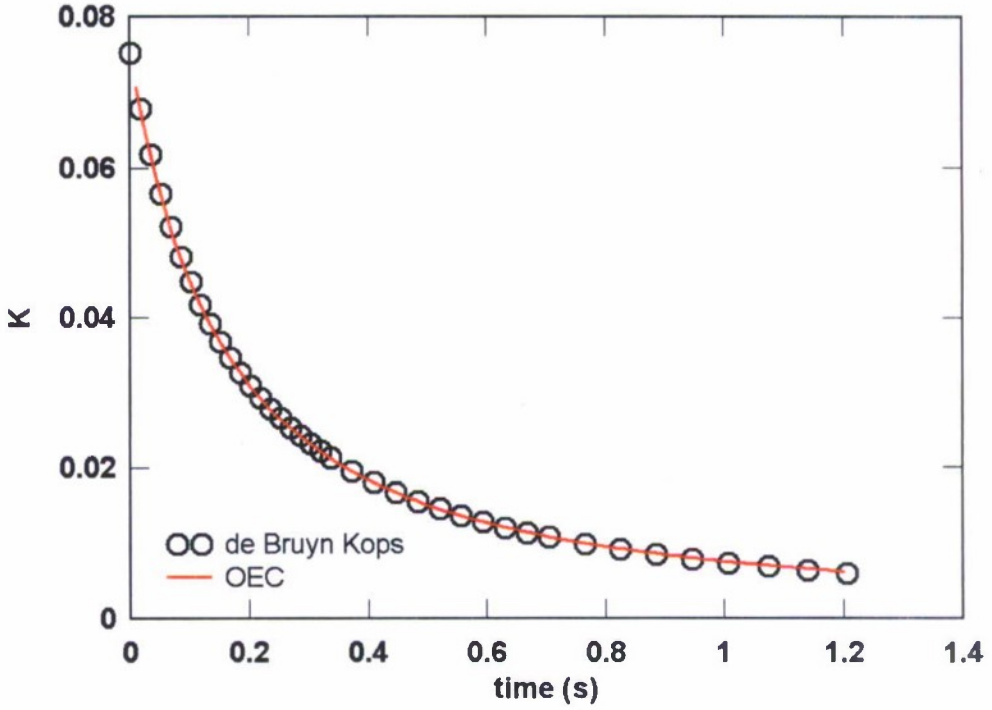

Figure 5: Isotropic, homogeneous decay compared to DNS data from de Bruyn Kops , *et al.* (1998).

Data from de Bruyn Kops, *et al.* (1998) was again employed for validation. As was expected, agreement between OEC and the DNS data was excellent, and more complex cases could be considered.

Perfecting the system rotation term

The system rotation term (previously $\hat{s}_l$, now B_l) was re-examined after long-term stability for shear cases such as Matsumoto, *et al.* (1991) came in to question. Several rotation term options were considered and their constants determined. The current rotation term is defined in as

$$B_i = \frac{1}{\tau_R}\left\{\frac{\frac{1}{N}\sum\left[\frac{\left(q_k\Omega_k^*\right)^2}{q^2}\right]}{C_S^K\overline{q^2}\,\overline{K}+C_S^\Omega\left(\Omega_k^*\right)^2}\right\}q_i \tag{42}$$

with $1/\tau_R = \left(\overline{K}\,\overline{q^2}\right)^{\frac{1}{2}}$ a decay constant, q_i the eddy orientation vector, $\Omega_i^* = \varepsilon_{ijk}\overline{u}_{k,j} + \Omega_i$ a modified system rotation vector, $\overline{K}$ the average (not per-eddy) kinetic energy, N the number of eddies in the simulation and constants C_S^K and C_S^Ω. Note the updated nomenclature. The model was then subjected to more complex flow situations such as rotating decay, a mixing layer, and several shear and strain cases.

Table 2: Initial conditions for Wigeland and Nagib (1978).

Wigeland & Nagib									
	A			B			C		
$\varepsilon(m^2/s^3)$	14.85	14.67	14.94	2.96	3.49	3.36	2.77	3.36	22.26
$K(m^2/s^2)$	0.098	0.0975	0.105	0.045	0.0462	0.051	0.029	0.033	0.096
$\nu(m^2/s)$	1.8e-5	1.8e-5	1.8e-5	1.8e-5	1.8e-5	1.8e-5	1.8e-5	1.8e-5	1.8e-5
Re_T	36	36	41	38	34	43	17	18	23
Ro_T	∞	7.52	1.78	∞	3.77	0.82	∞	5.09	2.9
Ω_i	**0**	**20**	**80**	**0**	**20**	**80**	**0**	**20**	**80**

Wigeland and Nagib (1978) provide data which test both rotating and non-rotating decay, as seen in Figure 6:

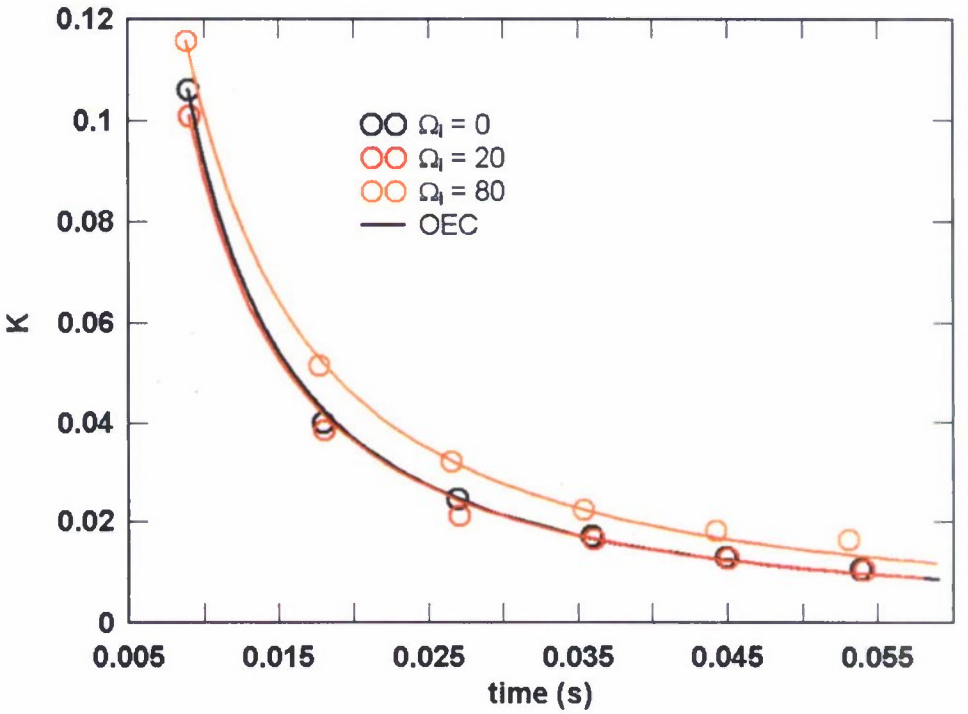

Figure 6: Rotating and non-rotating decay from Wigeland and Nagib, case A.

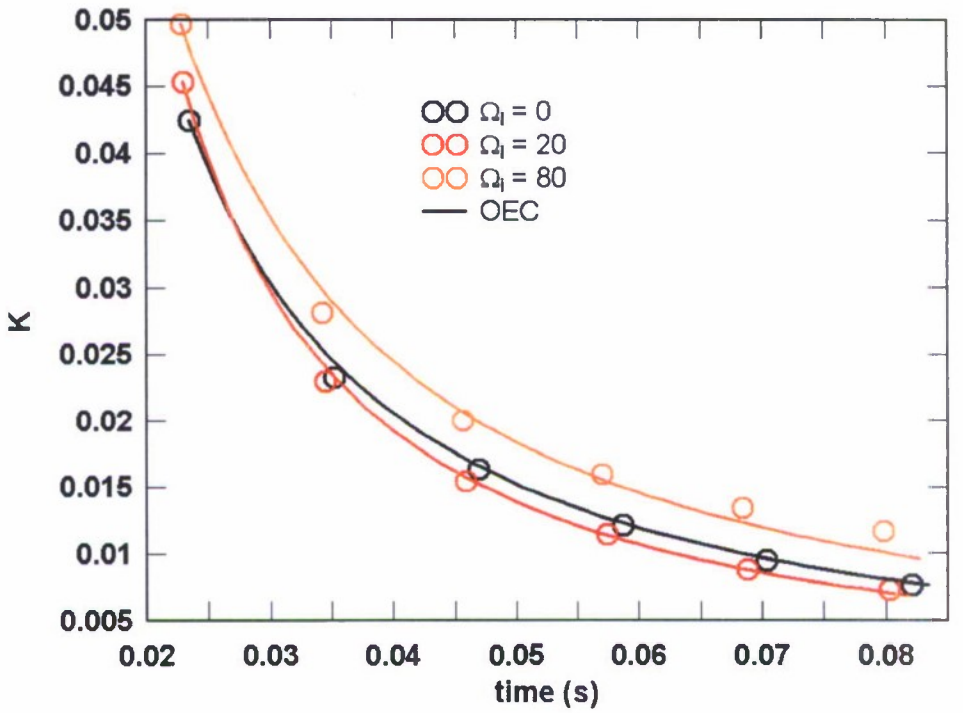

Figure 7: Rotating and non-rotating decay from Wigeland and Nagib, case B.

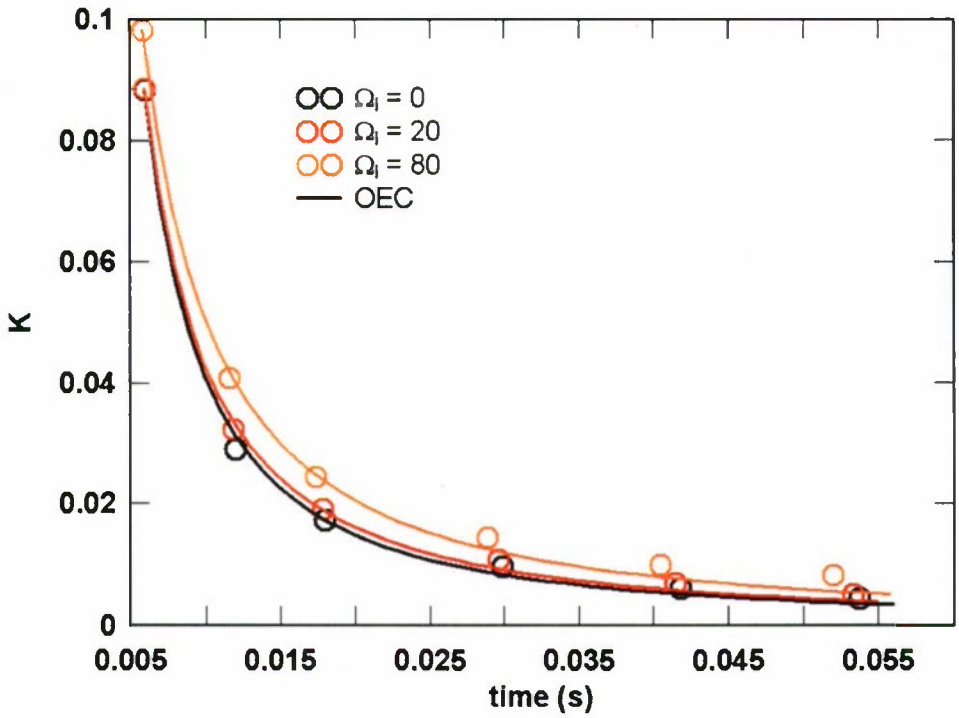

Figure 8: Rotating and non-rotating decay from Wigeland and Nagib, case C.

As Figure 6 through Figure 8 show, agreement is good across a range of Rossby and Reynolds numbers. Rotating decay was also tested with results from Jacquin, *et al.* (1990). Note that only the highest Reynolds number case is shown here as agreement at lower Reynolds numbers was excellent and tested extensively previously. Agreement with Jacquin's high Reynolds number data was excellent.

Table 3: Initial conditions for Jacquin's rotating decay.

Jacquin			
	A	B	C
$\varepsilon(m^2/s^3)$	11.73	16.43	30.93
$K(m^2/s^2)$	0.153	0.288	0.444
$\nu(m^2/s)$	1.51e-5	1.51e-5	1.51e-5
Re_T	127	281	457
Ro_T	1.22	0.91	1.10

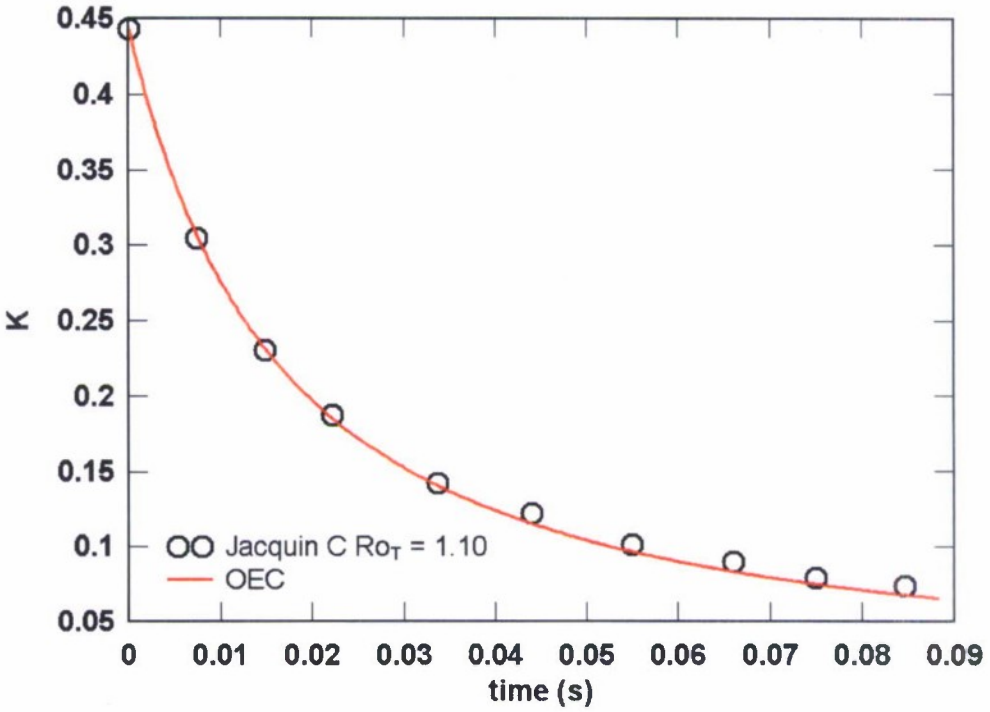

Figure 9: Rotating and non-rotating decay from Jacquin, *et al.* with $Ro_T = 1.10$ (case C).

Finally, data taken from Mansour, Cambon, and Speziale was also used to determine the performance of OEC's rotation terms:

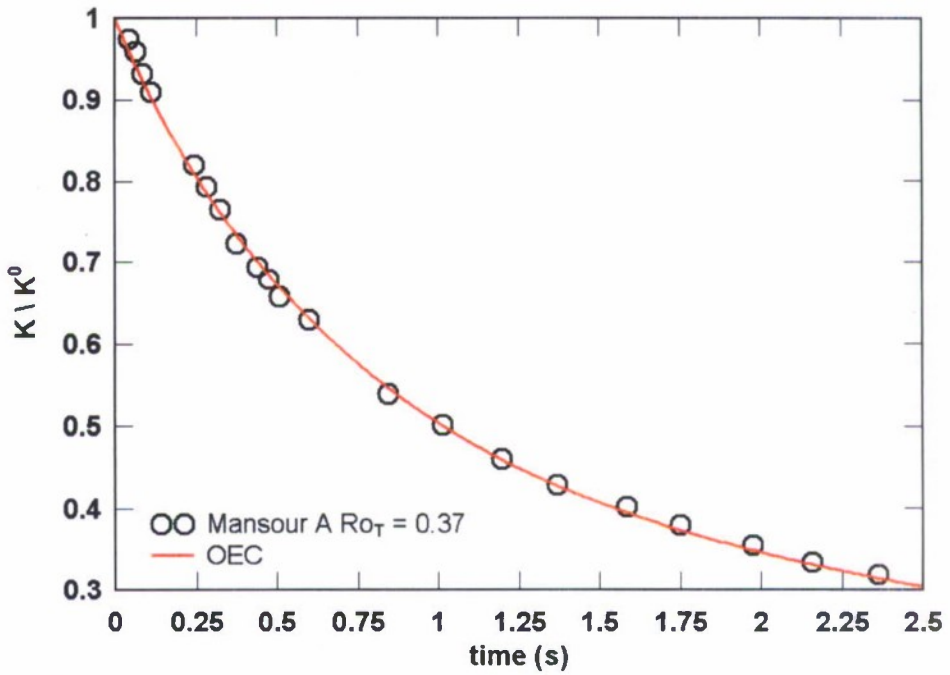

Figure 10: OEC compared to rotating isotropic decay data from Mansour, Cambon, and Speziale (A).

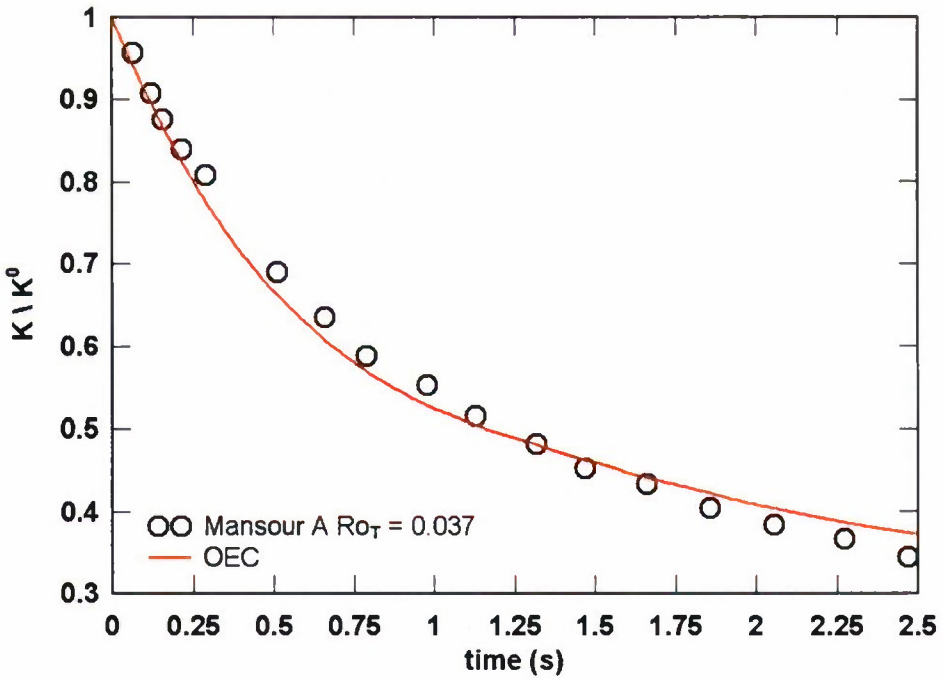

Figure 11: OEC compared to rotating isotropic decay data from Mansour, Cambon, and Speziale (B).

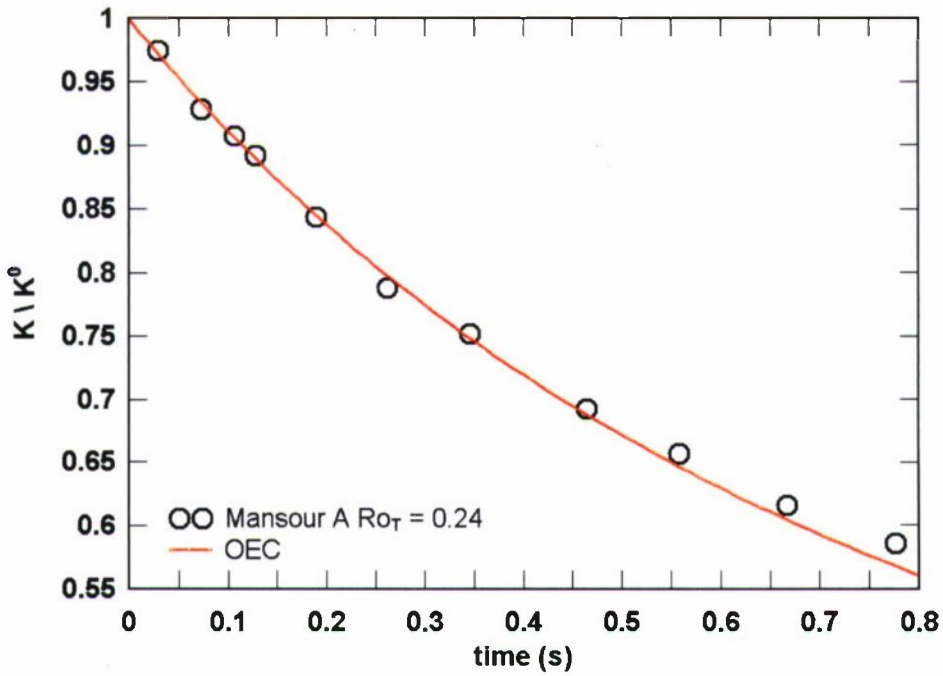

Figure 12: OEC compared to rotating isotropic decay data from Mansour, Cambon, and Speziale (C).

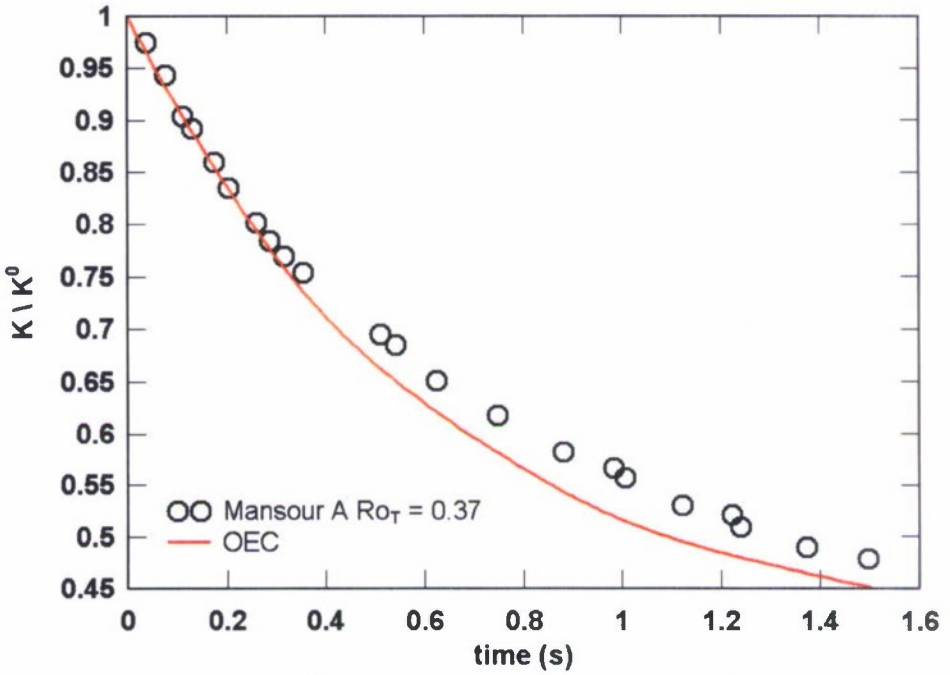

Figure 13: OEC compared to rotating isotropic decay data from Mansour, Cambon, and Speziale (D).

Table 4: Initial conditions for Mansour, *et al* rotating cases.

	Mansour, Cambon & Speziale			
	A	B	C	D
$\varepsilon(m^2/s^3)$	0.93		0.95	
$K(m^2/s^2)$	0.964		0.977	
$\nu(m^2/s)$	3.67e-2		1.49e-2	
Re_T	27.2		67.1	
Ro_T	0.37	0.037	0.24	0.1

The model agreed well with available data (mostly from direct numerical simulations) and mixing layer data from Winckelmans, Jeanmart, and Carati (2002) was used to test the model's ability to capture the decay of kinetic energy and dissipation which differs spatially. Kinetic energy results are shown in Figure 14 and dissipation results in Figure 15 . Carati's data is unique in a sense that we have access to both the kinetic energy and the dissipation rate. OEC's prediction of the decay of both the average kinetic energy $\overline{K}$ and average (calculated) dissipation

$$\overline{\varepsilon} = \frac{1}{N}\sum\left(q^2 K\right)\nu\alpha + \overline{K}^{\frac{3}{2}}\overline{|q_i|} \tag{43}$$

is quite close to Carati's at t = 0.171 seconds. However, the model seems to slightly over predict the kinetic energy at the later time and under predict the dissipation.

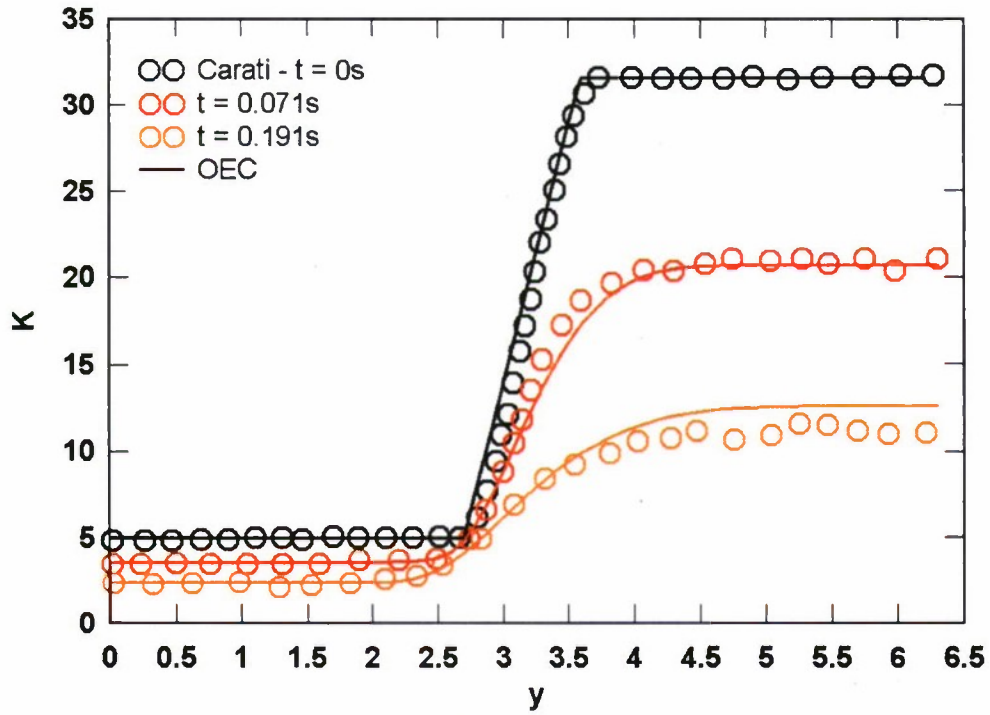

Figure 14: Decay of kinetic energy versus position at three different times from Carati, *et al.* (2002).

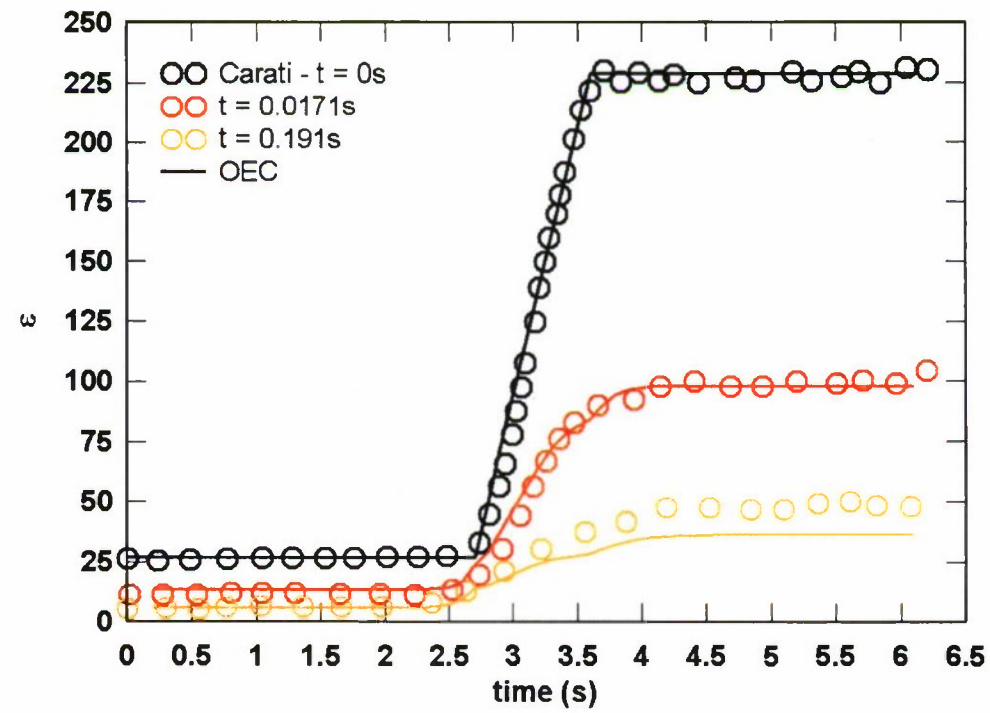

Figure 15: Decay of dissipation versus position at three different times from Carati, *et al.* (2002).

OEC in the Rapid Distortion Theory Limit

The addition of orientation information to OEC enables the model's unique ability to capture turbulence in extreme circumstances, such as those described by rapid distortion theory (RDT). Pope (2000) covers this subject in detail. Amongst the RDT cases considered and used for validation were the following: Axisymmetric expansion, akin to an expansion in a wind tunnel in transverse directions; axisymmetric contraction in which the turbulent flow is contracted in the transverse directions, plane strain, and finally shear. The four cases are summarized in Table 5:

Table 5: RDT cases used for testing OEC in FOAM.

	Axisymmetric contraction	Axisymmetric expansion	Plane Strain	Shear
R_{11}	S	$-2S$	S	0
R_{22}	$-\frac{1}{2}S$	S	$-S$	0
R_{33}	$-\frac{1}{2}S$	S	0	0
R_{12}	0	0	0	S
$S \equiv (2\bar{S}_{ij}\bar{S}_{ij})^{1/2}$	$\sqrt{3}S$	$2\sqrt{3}S$	$-2S$	$2S$

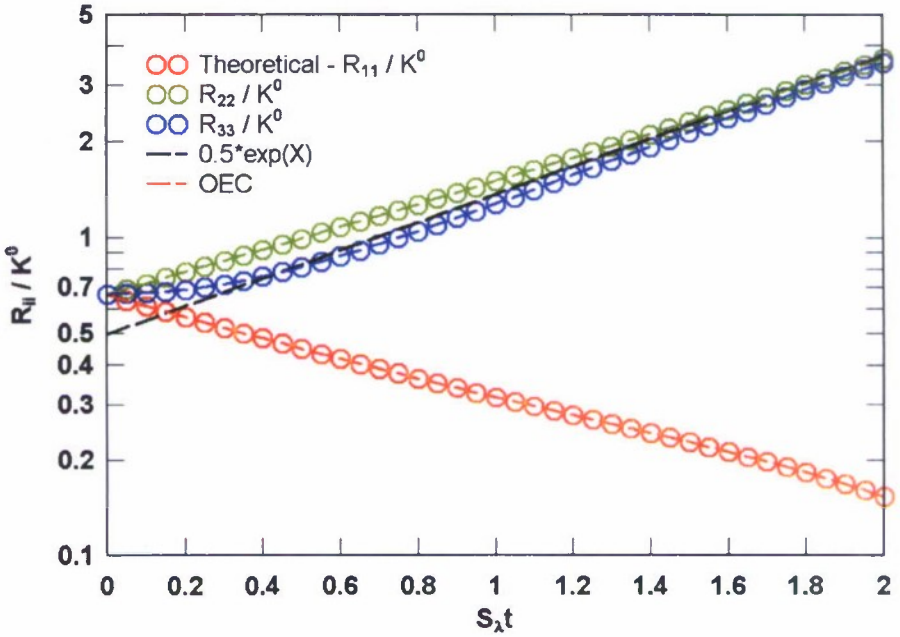

Figure 16: OEC subjected to plane strain and compared to theory (Pope 2000).

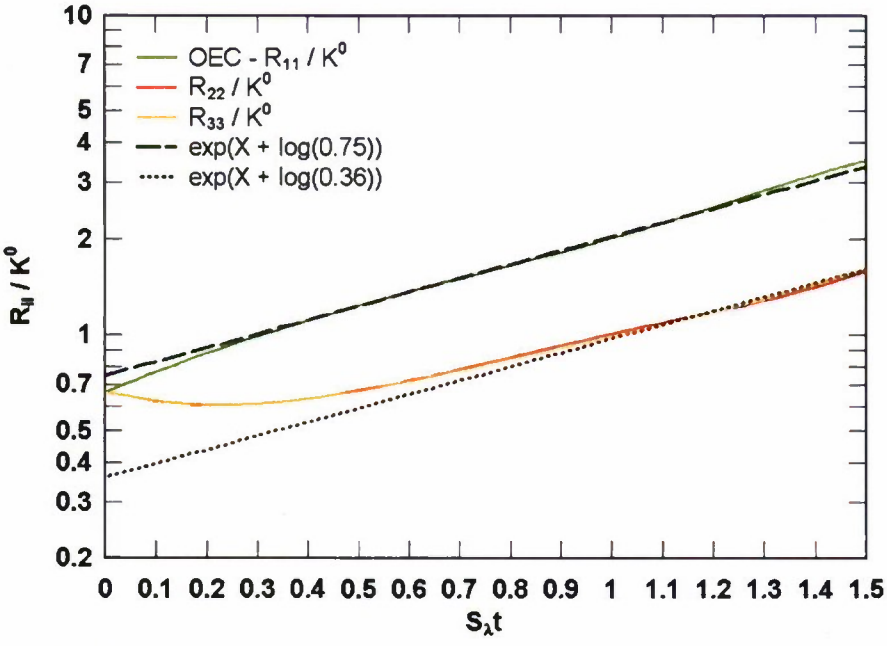

Figure 17: OEC subjected to axisymmetric expansion and compared to theory (Pope 2000).

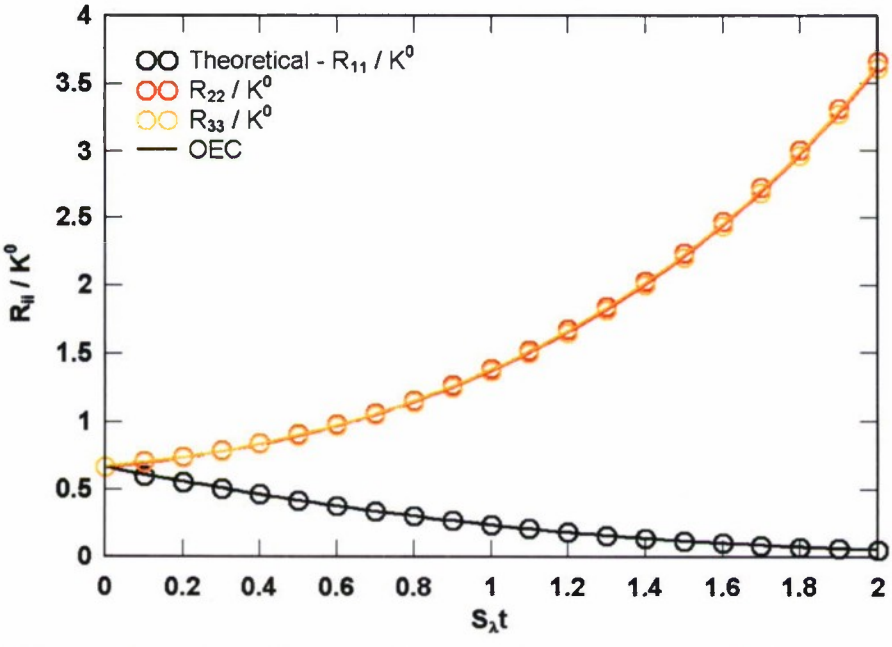

Figure 18: OEC subjected to axisymmetric expansion and compared to theory (Pope 2000).

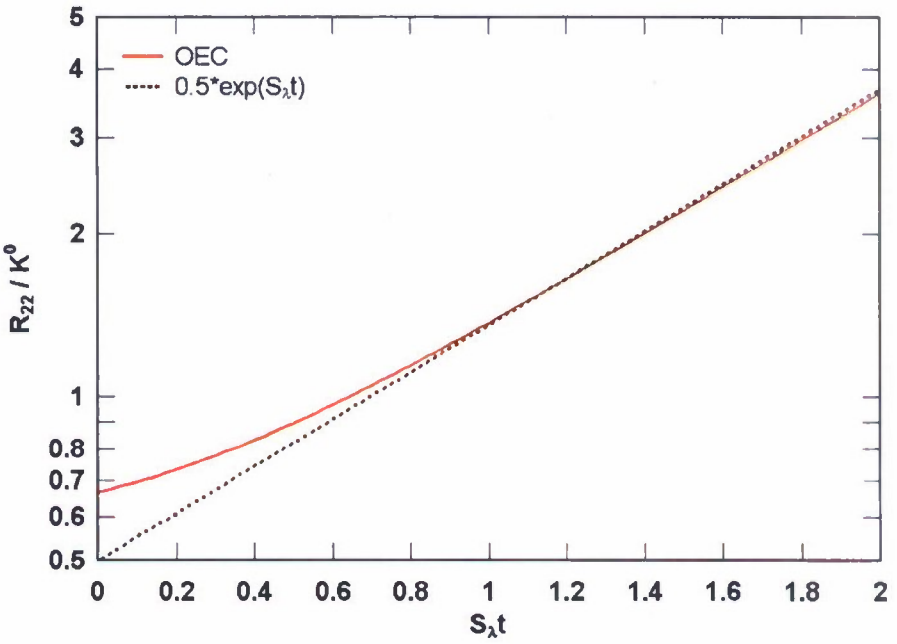

Figure 19: A closer look at the behavior of the normalized stress component R_{22} compared to theory (Pope 2000).

OEC in Shear Flow

After testing each term in the model, OEC was subjected to homogeneous turbulent shear flow in order to compare with data available from Matsumoto, Nagano, and Tsuji (1991) as well as L. Le Penven, J. N. Gence, and G. Comte-Bellot (1985). This provided a means of testing the model as a whole while remaining geometrically simple and not requiring wall boundary conditions.

Table 6: Summary of shear flow cases used to validate OEC

	Matsumoto		LePenven A	LePenven B
SK/ε	30.6	4.71	0.43	0.33
Re_T	18.18	152	612	846
Strain Tensor	$\begin{pmatrix} 0 & 28.28 & 0 \\ 0 & 0 & 0 \\ 0 & 0 & 0 \end{pmatrix}$	$\begin{pmatrix} 0 & 30 & 0 \\ 0 & 0 & 0 \\ 0 & 0 & 0 \end{pmatrix}$	$\begin{pmatrix} 5.48 & 0 & 0 \\ 0 & 1.99 & 0 \\ 0 & 0 & -7.47 \end{pmatrix}$	$\begin{pmatrix} 8.86 & 0 & 0 \\ 0 & -2.36 & 0 \\ 0 & 0 & 6.50 \end{pmatrix}$

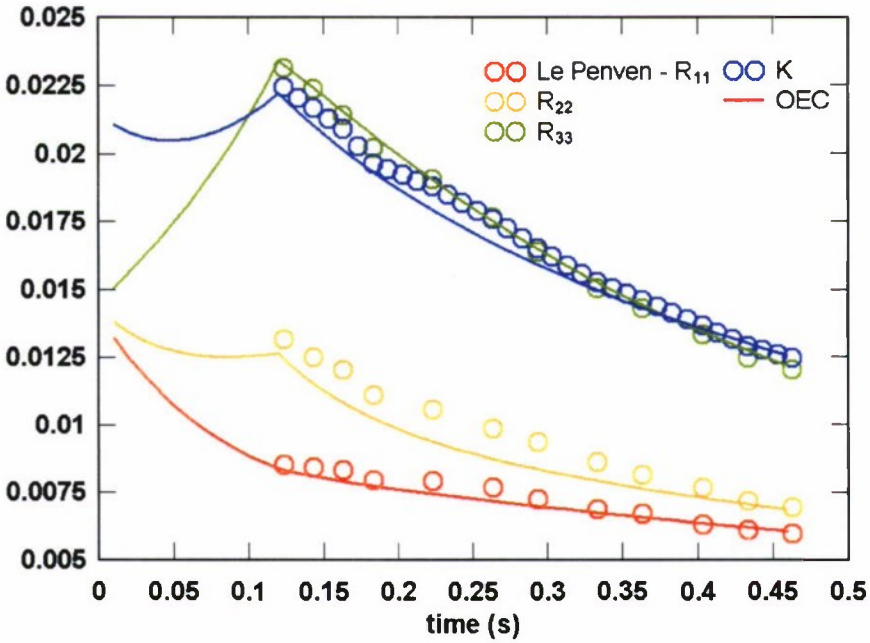

Figure 20: Comparison to data from L. Le Penven, J. N. Gence, and G. Comte-Bellot, case A.

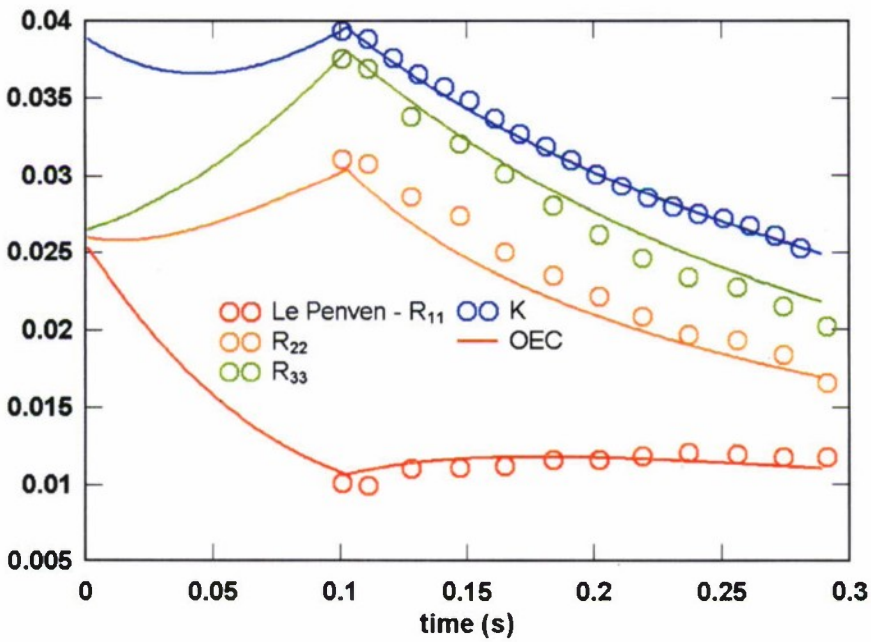

Figure 21: Comparison to data from L. Le Penven, J. N. Gence, and G. Comte-Bellot, case B.

Results for Matsumoto, *et al.* (1991) low Reynolds number flow, $Re_T = 18$, are shown in Figure 22:

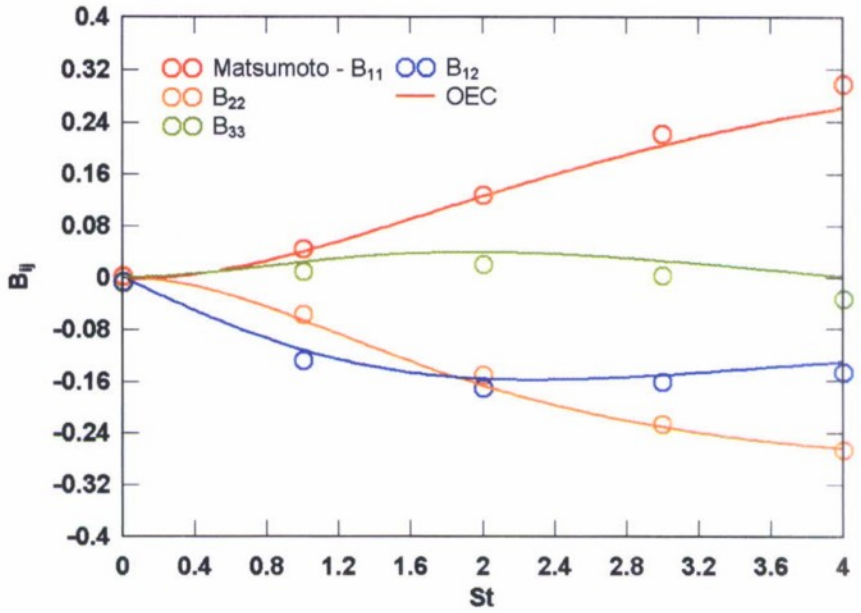

Figure 22: Shear data at a turbulent Reynolds number $Re_T = 18$ from Matsumoto, Nagano, and Tsuji who provide data for the time evolution of the anisotropy tensor. Time in non-dimensionalized by the shear, S.

The model agrees quite well with the data provided from Matsumoto, *et al.* (1991). Results for higher Reynolds number $Re_T = 152$ flow, for a much longer span of characteristic time scale *St*, is shown below in Figure 23:

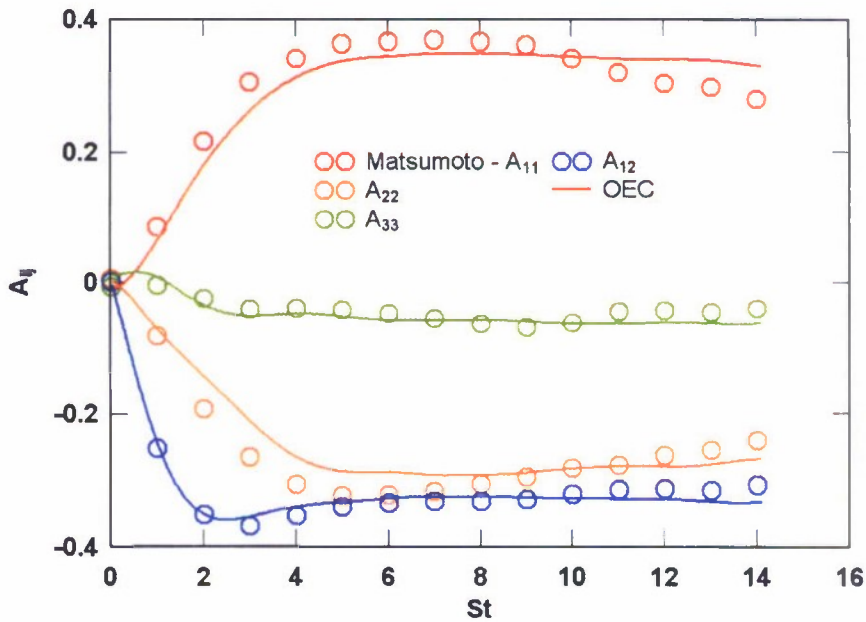

Figure 23: Shear data at a turbulent Reynolds number $Re_T = 152$ from Matsumoto, Nagano, and Tsuji who provide data for the time evolution of the anisotropy tensor A_{ij}.

Again, agreement is excellent with Matsumoto's data. With the successful benchmarking of OEC with Matsumoto's shear case, the model was ready for further development. Of course, solid boundaries are always a concern with RSTM-like models, and are currently a subject of intense research. Before tackling that problem, however, the problem of temporal stability will be addresses.

Temporal Stability

Increasing the temporal stability of the code was addressed next and a 3rd order low-storage Runge-Kutta time marching scheme was successfully implemented and tested in OpenFOAM. For temporal discretization, the program utilizes a three step Runge-Kutta time marching method (RK3), which is second order accurate. Denoting intermediate solution steps as $\tilde{y}$ and $\tilde{\tilde{y}}$, we arrive at the following low storage, second order accurate form of the hybrid RK3 found in the code:

$$\begin{aligned} \tilde{y}_{n+\frac{1}{2}} &= y_n + \left(\frac{1}{2}\Delta t\right)\cdot f\left(y_n\right) \\ \tilde{\tilde{y}}_{n+1} &= y_n + \left(\Delta t\right)\cdot f\left(\tilde{y}_{n+\frac{1}{2}}\right) \\ y_{n+1} &= \tilde{y}_{n+\frac{1}{2}} + \left(\frac{1}{2}\Delta t\right)\cdot f\left(\tilde{\tilde{y}}_{n+1}\right) \end{aligned} \tag{44}$$

where $\tilde{y}_{n+\frac{1}{2}}$ represents the intermediate velocity (flux), pressure, Reynolds stress, eddy vector, or kinetic energy information. The first step of RK3 uses the explicit Euler method to arrive at a solution at one half the time step. The code then uses this midpoint solution to leapfrog to the end of the time interval. Finally, it performs another Euler step to arrive at a solution at the next time step. The low storage method trades off accuracy for minimal storage. Only two arrays need be stored for any given calculation, the solution from the previous step, y_n, and the result of the previous intermediate step $\tilde{y}$ or $\tilde{\tilde{y}}$. Implementing this method in to OpenFOAM was done for OEC specifically, and not in a general form. OpenFOAM allows for runtime selection of time stepping schemes, but is currently limited to one step schemes such as explicit Euler or second order schemes such as Crank-Nicholson. As such, any higher order scheme such as RK3 must be added to FOAM.

As was the case with boundary conditions (discussed below), there are generally two approaches to implementing a new feature in FOAM. The first is to spend the effort of creating a generic, templated entity (in this case a time derivative scheme), fold this code in to the existing framework, and then call the method. While more attractive to the general user, the time required to do this is often not worth the reward. In this case, the RK3 scheme was "hard coded" in to OEC and employ's FOAM's

explicit Euler time derivative scheme for temporal sub-stepping. FOAM stores the previous values for a given entity (such as an eddy vector) making implementation easier. Old values can be easily recalled, and in certain circumstances FOAM's default behavior can be overridden using the ".storeOldTime()" function. This was especially useful when constructing the RK3 scheme in OpenFOAM as there are a good number of intermediate arrays to be stored for the Reynolds stress tensor, eddy vector, kinetic energy, and velocity at each cell for every eddy. Future work on OEC in OpenFOAM may include the development of a general Runge-Kutta time marching scheme for users of the model and the general public.

Solid Boundaries

After temporal stability issues were overcome, effort shifted to slip and no-slip boundary conditions. These are imperative for wall-bounded flows or flows over objects which are of paramount importance to engineers and are the focus of our current work. The model is currently being tested using benchmark cases such as turbulent Couette flow, turbulent channel (Poiseuille) flow and a backward facing step. In addition, more complex cases such as flow around an oblate spheroid have been considered. Preliminary work on turbulent flow ($Re = 5000$) over an oblate spheroid using OEC running in parallel on four processors is shown in Figure 24 and Figure 25 :

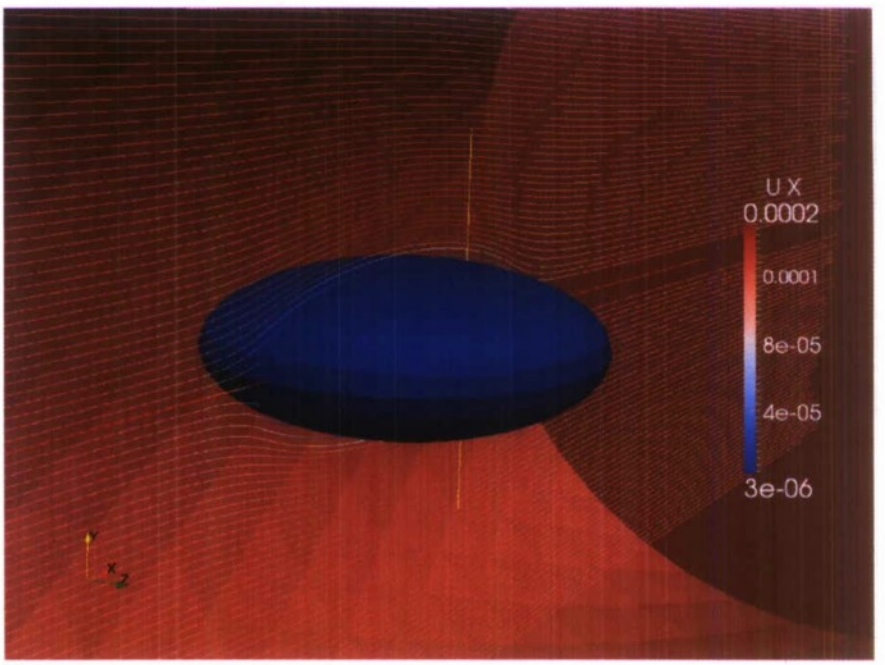

Figure 24: Velocity streamlines from turbulent flow over an oblate spheroid using the OEC model. The spheroid's surface is no-slip while the domain walls are zero gradient.

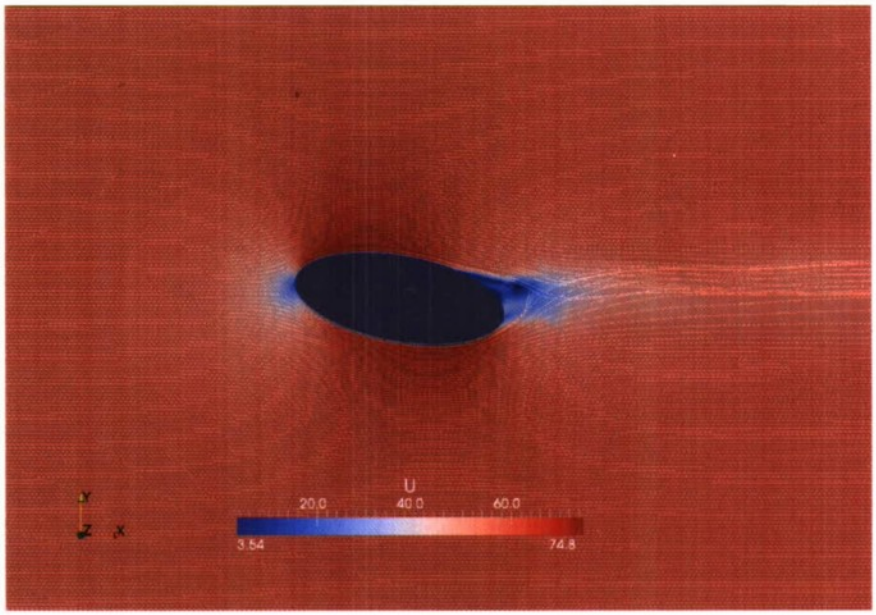

Figure 25: Velocity streamlines from turbulent flow over an oblate spheroid using the OEC model. The wake can be easily seen in this slice.

Trials continue with simulations over solid boundaries including turbulent Couette flow, turbulent channel flow, and flows over an oblate and prolate spheroid.

Modifications for near-wall stability

Unfortunately, as is the case with many Reynolds stress transport models (RSTM), problems arise when walls are introduced as both the Reynolds stress and kinetic energy become zero at the boundaries. In order to maintain stability at walls, the OEC model was recast to evolve the Reynolds stresses normalized by the kinetic energy, $R^*_{ij} = R_{ij} / K$. This necessitated an evolution equation for the kinetic energy K as well. The eddy orientation vector equation was unchanged. The new casting of the OEC model became:

$$\frac{\partial K}{\partial t} + \nabla \cdot \left(\bar{u}_j K \right) = -K \bar{u}_{k,i} - \frac{1}{3} \left(\alpha \cdot \nu q^2 + \tfrac{1}{\tau_R} \right) K + P^* K - A^* K + M^* K + \nabla (\nu + \nu_t) \nabla K \tag{45}$$

$$\frac{\partial R^*_{ij}}{\partial t} + \nabla \cdot \left(\bar{u}_k R^*_{ij} \right) = \left(P^*_{ij} - R^*_{ij} P^* \right) - \left(\alpha \nu q^2 + \tfrac{1}{\tau_R} \right) R^*_{ij} - \left(A^*_{ij} - R^*_{ij} A^* \right) + \left(M^*_{ij} - R^*_{ij} M^* \right) + \nabla \cdot \left(\nu + \nu_t \right) \nabla R^*_{ij} \tag{46}$$

noting that the equation for q_t is unaltered and that $C_p = 2$. The first equation above evolves the per-eddy kinetic energy K. In Equations (45) and (46), P_{ij}^* is the same as P_{ij} except it involves R_{ij}^* as opposed to R_{ij} which is true for M_{ij}^* as well. $P^* = 0.5P_{ii}^*$ and similarly $M^* = 0.5M_{ii}^*$. The Reynolds stress return to isotropy term A_{ij}^* is slightly different from the one found in the original OEC model, as shown in below:

$$A_{ij}^* = \frac{1}{\tau_R}\left(\frac{C_{RR}^{Up}}{1+C_{RR}^{Dn}\left(\frac{\nu}{\nu_T}\right)}\right)\left[R_{ij}^* - \frac{\overline{K}}{K}\left(\delta_{ij} - \frac{q_i q_j}{\hat{q}^2}\right)\right] \tag{47}$$

noting that the average kinetic energy $\overline{K}$ is normalized by the local (per-eddy) kinetic energy K. Evolving R_{ij}^* allows the per-eddy Reynolds stress R_{ij} to be calculated via $R_{ij} = R_{ij}^* K$ which does not present problems when $K = 0$. Once complete, the new q_t, K, R_{ij}^* ("qkRStar") casting of OEC was tested using the same cases that were employed for the original q_t, R_{ij} ("qR") model. Results from the two models matched closely.

Near-wall behavior of turbulent eddies

In addition to ensuring stability at walls, it is necessary to ensure that the eddies (i.e. the eddy orientation vectors and subsequently the per-eddy Reynolds stresses) interact with the region near a wall (the large-scale damping effect). In addition, the eddies must align themselves properly to ensure they are not embedded within the wall:

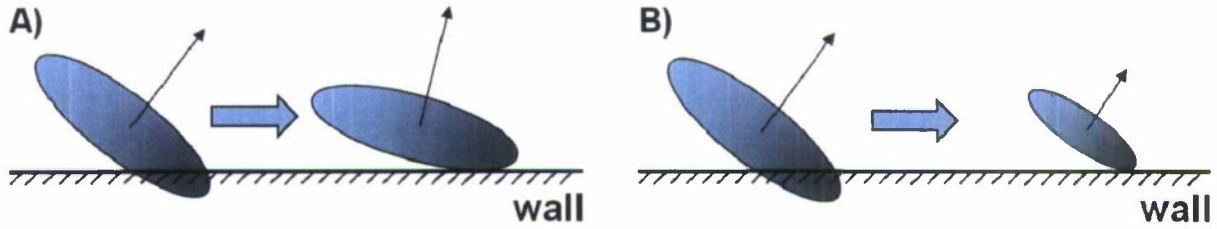

Figure 26: Eddies that intersect solid boundaries must be rotated out of the way. A) This rotation preserves the magnitude of the eddy, which does not affect the near-wall dissipation. B) This scaling achieves the same goal, but affects the near-wall dissipation.

As such, an additional term is effectively added to (although not explicitly stated in) both the q_t and R_{ij} or R_{ij}^* equations. One method rotates the eddy vector away from the wall while maintaining its magnitude, shown in Figure 26 A. This method does not affect the near-wall dissipation by maintaining the length scale (eddy vector magnitude). A second method, illustrated in Figure 26 B, changes the magnitude of the eddy vector, which of course affects the eddy vector magnitude (by decreasing it) and thus the near wall dissipation. For the first case, the angle between the old and

new eddy vectors is calculated and Rodrigues' rotation formula applied to align R_{ij} or R_{ij}^* in with the new eddy vector incompressibility (i.e. orthogonality between q_i and R_{ij} or R_{ij}^*). Implementation details and the algorithm employed to perform this rotation are discussed later.

The presence of walls in a turbulent flow imparts so-called non-local effects on the flow, specifically affecting turbulent redistribution. Durbin (2001) discusses two of the most common methods that near-wall modeling is achieved, pressure echo and elliptical relaxation. Both methods seek to alter turbulence quantities near to but not at a wall in order that the model return more realistic results. Solid boundaries tend to cause regions of strong inhomogeneity, production and shear. The region acts to suppress wall-normal turbulence, which can have a drastic effect on the nature of the near-wall Reynolds stress tensor. Unfortunately, most RSTMs lack a mechanism to ensure this behavior, thus special consideration must be made. OEC is no different, and the aforementioned "near wall rotation" of the eddy vectors is this model's novel solution to the problem. Great care must be taken when attempting to use RST models near solid boundaries where the velocity and Reynolds stresses tend to zero. At the moment, wall functions and damping are the most popular methods employed to handle solid boundaries. Not only is it imperative that the value at the boundary be prescribed, but the model must also behave properly as it *approaches* the wall, meaning the model's asymptotic behavior must be considered. If the fluctuating velocity is considered to be a smooth function of the distance from the solid boundary y, then it can be expanded as a Taylor series, *viz.* $u_i = p_i + q_i y + r_i y^2$ with p_i, q_i, and r_i functions of the wall-tangent directions, and truncating higher order terms. If the velocity at the wall is zero, $u_i(y=0)=0$, then $p_i = 0$ which implies u_1 and u_3 (in the tangential x and z directions, respectively) approach the boundary like y. Furthermore, if continuity is invoked, it is found that velocity in the wall normal direction u_2 approaches the wall like y^2. Using this information, the near wall asymptotic behavior of the individual Reynolds stress tensor components can be assessed: $\overline{u_1 u_1}$, $\overline{u_3 u_3}$, and $\overline{u_1 u_3}$ will approach like y^2. $\overline{u_1 u_2}$ and $\overline{u_2 u_3}$ will go like y^3, and $\overline{u_2 u_2}$ like y^4 (Durbin 2001, Pope 2000). It is not trivial to ensure this behavior, and is an area of active research for the Oriented Eddy Collision model. The near-wall region creates other difficulties: the highest shear rate is often located at a solid wall, and the normal velocity being forced to zero at the wall tends to affect the flow away from the wall via pressure (often called ``wall blocking'').

Another subtlety which arises when implementing wall boundary conditions for the eddy orientation vectors q_i. At a shear free (slip) wall, the eddies align themselves to be tangential to (in the plane of) the wall and the magnitude of the eddy should remain unchanged. At a no-slip wall, however, the eddy size should approach zero. Considering q_i has units of 1 / length, an eddy of zero size would correspond to a q_i of infinity. In order to avoid this problem, the OEC model has once again been re-cast to

evolve the eddy length itself, $L_i = q_i / q^2$, which has units of length and thus can be set to zero at no slip walls. This will be covered in the next section.

Avoiding Troublesome Boundary Conditions

Numerous changes have been made to both the OEC model and its nomenclature, most of which centered on casting the model in such a way that it would be stable at solid boundaries and numerically tractable. As mentioned previously, evolving a quantity like the eddy vector q_i (hats will be dropped hereafter) is troublesome as the quantity goes to infinity at a solid boundary if the eddy length scale goes to zero. This is a problem separate from near-wall local effect discussed in the previous section. Since its initial casting and subsequent modifications with a normalized Reynolds stress tensor, several changes have been made to the nomenclature as well as a symbolic representation of the near-wall rotation performed on the eddies. The original eddy orientation evolution equation, in its current form:

$$\frac{Dq_i}{Dt} = -q_k \bar{u}_{k,i} - \frac{1}{3}\left(\alpha \nu \overline{q^2} + \frac{1}{\tau_R}\right) q_i - (A_i + B_i) + \frac{1}{3}\left[(\nu + \nu_t) q_{i,k}\right]_{,k} + W_i \tag{48}$$

with near-wall rotation term W_i. The current form of the return to isotropy term for the eddy vectors A_i:

$$A_i = \frac{C_{A_i}}{\tau_R}\left\{\frac{\nu_T}{\nu_T + C_A^{Dn}\nu}\right\}\left[3N_{ki} - \delta_{ki}\right] q_k \tag{49}$$

with the isotropy tensor $N_{ki} = \overline{q_i q_k} / \overline{q^2}$ determining the departure of the eddy vectors from theory original (spherical) isotropic condition. The current system rotation term B_i is defined as:

$$B_i = \frac{1}{\tau_R}\left\{\frac{\overline{\left(q_k \Omega_k^*\right)^2 / q^2}}{20.0\overline{q^2}\,\overline{K} + 0.25\left(\Omega_k^*\right)^2}\right\} q_i \tag{50}$$

recalling the time scale is defined as

$$\frac{1}{\tau_R} = \left(\overline{K}\,\overline{q^2}\right)^{\frac{1}{2}} \tag{51}$$

and the turbulent viscosity as

$$\nu_T = \left(\frac{\overline{K^2}}{\overline{Kq^2}}\right)^{\frac{1}{2}} \tag{52}$$

Note that, for simplicity's sake, the hats (which previously indicated a "per-eddy" quantity) have been dropped. In addition, the previous rotation constants have been hard coded as $C_S^K = 20.0$ and $C_S^\Omega = 0.25$. The corresponding Reynolds stress tensor is currently posed as

$$\begin{aligned}\frac{DR_{ij}}{Dt} &= \left[\overline{u}_{i,k} + \left(\frac{q_i q_l}{q^2} - \delta_{il}\right) 2\overline{u}^*_{l,k}\right] R_{kj} + \left[\overline{u}_{j,k} + \left(\frac{q_j q_l}{q^2} - \delta_{jl}\right) 2\overline{u}^*_{l,k}\right] R_{ki} \\ &-\left(\alpha\nu\overline{q^2} + \frac{1}{\tau_R}\right) R_{ij} - A_{ij} + M_{ij} + \left[\left(\nu + \nu_t\right) R_{ij,k}\right]_{,k} \\ &-D\left(\nu + \nu_t\right)\left[\frac{R_{ij}}{K}\right]_{,k} (K)_{,k} - E\left(\nu + \nu_t\right)\frac{(K)_{,k}}{K}\frac{(K)_{,k}}{K} R_{ij} + W_{ij}\end{aligned} \tag{53}$$

with near wall rotation term W_{ij} responsible for rotating the Reynolds stress tensor, using Rodriguez's' rotation formula, to be aligned with the rotated near-wall eddy. The return to isotropy term for the Reynolds stress tensor, now written A_{ij}, takes its final form as

$$A_{ij} = \frac{C_{A_{ij}}}{\tau_R}\left\{\frac{\nu_T}{\nu_T + C_A^{Dn}\nu}\right\}\left[R_{ij} - \overline{K}\left(\delta_{ij} - \frac{q_i q_j}{q^2}\right)\right] \tag{54}$$

noting the change in nomenclature for the two return constants $C_{A_{ij}}$ and C_A^{Dn}. It is important to note that one return constant was eliminated, and C_A^{Dn} is common to both the eddy evolution equation and the Reynolds stress equation. In fact, all model constants remain consistent through the various versions presented here. A term is required to maintain orthogonality between the eddy vector and the Reynolds stress tensor (a condition which is also enforced by the near wall rotation term if it acts upon a given eddy vector and stress tensor in the domain). This term is written as

$$M_{ij} = \left(R_{lj}\frac{q_i}{q^2} + R_{li}\frac{q_j}{q^2}\right)\left(A_l + B_l\right) \tag{55}$$

with A_l and B_l the eddy vector return to isotropy and system rotation terms defined above. D and E are numerical constants, currently set to D = 2 and E = 0.

As was mentioned previously, the requirement of infinite boundary conditions applied to the eddy orientation vectors q_i led to the re-casting of OEC in terms of $L_i = q_i / q^2$ which has solid boundary conditions of $L_i = 0$. Note that a hat $\hat{}$ now

indicates a model quantity based on L_i rather than q_i. The evolution equation for the new eddy vector:

$$\frac{DL_i}{Dt} = -\left(\delta_{in} - 2\frac{L_n L_i}{L^2}\right)\left(L_k \bar{u}_{k,n}\right) + \frac{1}{3}\left(\alpha\nu\overline{\left(\frac{1}{L^2}\right)} - 2\nu\frac{|L|_{,k}|L|_{,k}}{L^2} + \frac{1}{\hat{\tau}_R}\right)L_i$$
$$-\left(\delta_{in} - 2\frac{L_n L_i}{L^2}\right)\left(\hat{A}_n + \hat{B}_n\right) + \tfrac{1}{3}\left[(\nu + \hat{\nu}_T)L_{i,k}\right]_{,k} + W_n \tag{56}$$

with W_n once again representing the near wall rotation term, which will be discussed later. Similar to the original form of the model, the return model is cast as such, noting that additional tuning using high Reynolds number shear flow from Matsumoto was employed to remove a tuning constant from the numerator:

$$\hat{A}_n = \frac{C_{A_i}}{\hat{\tau}_R}\left\{\frac{\hat{\nu}_T}{\hat{\nu}_T + C_A^{Dn}\nu}\right\}\left[3\hat{N}_{kn} - \delta_{kn}\right]L_k \tag{57}$$

noting the isotropy tensor $\hat{N}_{kn}$ is now defined as

$$\hat{N}_{kn} = \overline{\left(\frac{L_n L_k}{\left(L^2\right)^2}\right)} \Big/ \overline{\left(\frac{1}{L^2}\right)} \tag{58}$$

and the turbulent viscosity is cast as

$$\hat{\nu}_T = \left(\frac{\overline{K^2}}{\overline{\left(K\frac{1}{L^2}\right)}}\right)^{\frac{1}{2}} \tag{59}$$

The time scale is now written

$$\frac{1}{\hat{\tau}_R} = \left(\overline{K}\,\overline{\left(\frac{1}{L^2}\right)}\right)^{\frac{1}{2}} \tag{60}$$

The system rotation term for the L_i-based model becomes

$$\hat{B}_n = \frac{1}{\hat{\tau}_R}\left\{\frac{\overline{\left(L_k\Omega_k^*\right)^2/L^2}}{20.0\overline{\left(\frac{1}{L^2}\right)}\,\overline{K}+0.25\left(\Omega_k^*\right)^2}\right\}L_n \tag{61}$$

Note that $\frac{1}{3}\left(\alpha\nu\overline{\left(\frac{1}{L^2}\right)}-2\nu\frac{|L|_{,k}|L|_{,k}}{L^2}+\frac{1}{\hat{\tau}_R}\right)L_i$ above is an approximation. The exact derivation (or conversion) from the q_i-based model to the L_i-based model returns a dissipation term similar to that in the original casting of the model, namely $\frac{1}{3}\left(\alpha\nu\overline{\left(\frac{1}{L^2}\right)}+\frac{1}{\hat{\tau}_R}\right)L_i$ with several additional terms added the L_i evolution equation:

$$-\frac{2}{3}\left(\nu+\hat{\nu}_T\right)\frac{1}{L^2}\left(L^2\right)_{,k}L_{i,k}+\frac{2}{3}\left(\nu+\hat{\nu}_T\right)L^2\left\{\left(\frac{L_n}{L^2}\right)_{,k}\left(\frac{L_n}{L^2}\right)_{,k}\right\}L_i \tag{62}$$

These terms may be of some significance near solid boundaries and are the subject of future work. With the above model for the eddy length scale L_i, a corresponding model for the Reynolds stress tensor, now based on L_i, can be constructed:

$$\begin{aligned}\frac{DR_{ij}}{Dt} &= \left[\overline{u}_{i,k}+\left(\frac{L_iL_l}{L^2}-\delta_{il}\right)2\overline{u}^*_{l,k}\right]R_{kj}+\left[\overline{u}_{j,k}+\left(\frac{L_iL_l}{L^2}-\delta_{jl}\right)2\overline{u}^*_{l,k}\right]R_{ki}\\ &-\left(\alpha\nu\overline{\left(\frac{1}{L^2}\right)}+\frac{1}{\hat{\tau}_R}\right)R_{ij}-\hat{A}_{ij}+\hat{M}_{ij}+\left[\left(\nu+\hat{\nu}_t\right)R_{ij,k}\right]_{,k}\\ &-D\left(\nu+\hat{\nu}_t\right)\left[\frac{R_{ij}}{K}\right]_{,k}(K)_{,k}-E\left(\nu+\hat{\nu}_t\right)\frac{(K)_{,k}}{K}\frac{(K)_{,k}}{K}R_{ij}+W_{ij}\end{aligned} \tag{63}$$

Note the similarities between the version of the stress tensor evolution equation based on the original eddy vector q_i and its current form. Now, rather than denoting local, "per-eddy" quantities with a hat, we denote quantities based on the new eddy length scale L_i with a hat. The return to isotropy of the Reynolds stresses based on L_i is written as

$$\hat{A}_{ij} = \frac{C_{A_{ij}}}{\hat{\tau}_R}\left\{\frac{\hat{\nu}_T}{\hat{\nu}_T+C_A^{Dn}\nu}\right\}\left[R_{ij}-\overline{K}\left(\delta_{ij}-\frac{L_iL_j}{L^2}\right)\right] \tag{64}$$

and the corresponding orthogonality term

$$\hat{M}_{ij} = \left(R_{lj}L_i + R_{li}L_j\right)\left(\hat{A}_l + \hat{B}_l\right) \tag{65}$$

As was discussed in the previous section, a version of the model was also formulated for the evolution of the Reynolds stress tensor normalized by the kinetic energy, $R_{ij}^* \equiv R_{ij} / K$ where the star notation indicates that the stresses have been normalized. The current version of R_{ij}^* based on the original eddy vector q_i:

$$\begin{aligned}\frac{DR_{ij}^*}{Dt} &= \left[\overline{u}_{i,k} + \left(\frac{q_i q_l}{q^2} - \delta_{il}\right)2\overline{u}_{l,k}^*\right]R_{kj}^* + \left[\overline{u}_{j,k} + \left(\frac{q_j q_l}{q^2} - \delta_{jl}\right)2\overline{u}_{l,k}^*\right]R_{ki}^* \\ &-\left\{\left[\overline{u}_{n,k} + \left(\frac{q_n q_l}{q^2} - \delta_{nl}\right)2\overline{u}_{l,k}^*\right]R_{kn}^*\right\}R_{ij}^* - A_{ij}^* + M_{ij}^* + \left[\left(\nu + \nu_t\right)R_{ij,k}^*\right]_{,k} \\ &+(2-D)\left(\nu + \nu_t\right)\left[R_{ij}^*\right]_{,k}\frac{(K)_{,k}}{K}\end{aligned} \tag{66}$$

with the return to isotropy term defined as

$$A_{ij}^* = \frac{C_{A_{ij}}}{\tau_R}\left\{\frac{\nu_T}{\nu_T + C_A^{Dn}\nu}\right\}\left[R_{ij}^* - \left(\delta_{ij} - \frac{q_i q_j}{q^2}\right)\right]\left(\frac{\overline{K}}{K}\right) \tag{67}$$

and the orthogonality term

$$M_{ij}^* = \left(R_{lj}^*\frac{q_i}{q^2} + R_{li}^*\frac{q_j}{q^2}\right)(A_l + B_l) \tag{68}$$

Note that model terms based on the normalized Reynolds stress tensor R_{ij}^* also carry with them an asterisk *. Employing a normalized stress tensor

$$\begin{aligned}\frac{DK}{Dt} &= \left[\overline{u}_{i,k} + \left(\frac{q_i q_l}{q^2} - \delta_{il}\right)2\overline{u}_{l,k}^*\right]R_{ki} - \left(\alpha\nu\overline{q^2} + \frac{1}{\tau_R}\right)K - \frac{1}{2}A_{ii} + \frac{1}{2}M_{ii} \\ &+\left[\left(\nu + \nu_T\right)K_{,k}\right]_{,k} - E\left(\nu + \nu_T\right)\frac{(K)_{,k}(K)_{,k}}{K}\end{aligned} \tag{69}$$

As a fourth and final version of the OEC model, a version which combined the new eddy vector L_i and the normalized Reynolds stress tensor R_{ij}^* was created in hopes that the two variations would provide the most stability near solid boundaries:

$$\begin{aligned}\frac{DR_{ij}^*}{Dt} &= \left[\overline{u}_{i,k} + \left(\frac{L_i L_l}{L^2} - \delta_{il}\right) 2\overline{u}_{l,k}^*\right] R_{kj}^* + \left[\overline{u}_{j,k} + \left(\frac{L_j L_l}{L^2} - \delta_{jl}\right) 2\overline{u}_{l,k}^*\right] R_{ki}^* \\ &- \left\{\left[\overline{u}_{n,k} + \left(\frac{L_n L_l}{L^2} - \delta_{nl}\right) 2\overline{u}_{l,k}^*\right] R_{kn}^*\right\} R_{ij}^* - \hat{A}_{ij}^* + \hat{M}_{ij}^* + \left[\left(\nu + \hat{\nu}_t\right) R_{ij,k}^*\right]_{,k} \\ &+ (2 - D)\left(\nu + \hat{\nu}_t\right)\left[R_{ij}^*\right]_{,k} \frac{(K)_{,k}}{K}\end{aligned} \tag{70}$$

where once again D and is a numerical constant set to D = 2, this zeroing final term in the evolution equation and avoiding potential numerical stability issues. The return to isotropy term for the Reynolds stresses corresponding to the normalizes stress tensor model based on L_i:

$$\hat{A}_{ij}^* = \frac{C_{A_{ij}}}{\hat{\tau}_R}\left\{\frac{\hat{\nu}_T}{\hat{\nu}_T + C_A^{Dn}\nu}\right\}\left[R_{ij}^* - \left(\delta_{ij} - \frac{L_i L_j}{L^2}\right)\right]\left(\frac{\overline{K}}{K}\right) \tag{71}$$

with the orthogonality term written as

$$\hat{M}_{ij}^* = \left(R_{lj}^* L_i + R_{li}^* L_j\right)\left(\hat{A}_l + \hat{B}_l\right) \tag{72}$$

As was the case with the previous normalized stress tensor variant of OEC, an evolution equation for the kinetic energy K is required. In this case, this equation is constructed using the eddy length scale L_i:

$$\begin{aligned}\frac{DK}{Dt} &= \left[\overline{u}_{i,k} + \left(\frac{L_i L_l}{L^2} - \delta_{il}\right) 2\overline{u}_{l,k}^*\right] R_{ki} - \left(\alpha\nu\overline{\left(\frac{1}{L^2}\right)} + \frac{1}{\hat{\tau}_R}\right) K - \frac{1}{2}\hat{A}_{ii} + \frac{1}{2}\hat{M}_{ii} \\ &+ \left[\left(\nu + \hat{\nu}_T\right) K_{,k}\right]_{,k} - E\left(\nu + \hat{\nu}_T\right)\frac{(K)_{,k}(K)_{,k}}{K}\end{aligned} \tag{73}$$

The above four versions of the Oriented Eddy Collision model constitute the most current version of the model under development in OpenFOAM. Considering the difficult nature of capturing such a flow, the high Reynolds number Matsumoto case was used to compare the performance of the each model:

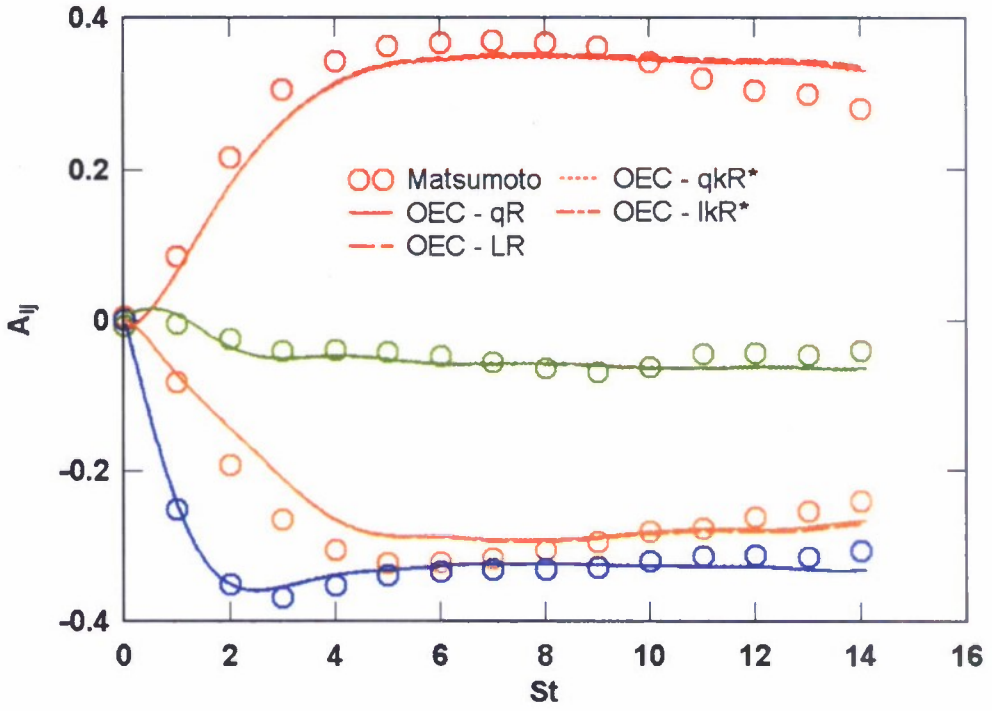

Figure 27: Taking another look at the Matsumoto ReT = 152 shear case, this time comparing all four model variants presented above. All four models show excellent agreement.

As seen above in Figure 27, the three additional models match the original "qR": "qkR*", which normalizes the stress tensor by the kinetic energy and has a transport equation for the kinetic energy, "LR" which used the eddy length vector L_i rather than the original q_i, and "lkR*"which employs both the eddy length vector L_i and the normalized stress tensor $R_{ij}^* = R_{ij} / K$.

The terms preceded by D and E are relatively new to the model (as compared to previous versions) and warrant discussion. The first involves the gradient of a Reynolds stress tensor. For models without normalized stress tensor these terms are

$$-D\left(\nu+\nu_t\right)\left[\frac{R_{ij}}{K}\right]_{,k}(K)_{,k} \tag{74}$$

and

$$-E\left(\nu+\nu_t\right)\frac{(K)_{,k}}{K}\frac{(K)_{,k}}{K}R_{ij} \tag{75}$$

in the Reynolds stress equation (for both models based on q_i and L_i). For those involving the normalized Reynolds stress tensor R_{ij}^*, the term of interest in the Reynolds stress equation is

$$(2-D)(\nu+\nu_t)\left[R_{ij}^*\right]_{,k}\frac{(K)_{,k}}{K} \tag{76}$$

The "extra" term in the kinetic energy equation is

$$-E(\nu+\hat{\nu}_T)\frac{(K)_{,k}(K)_{,k}}{K} \tag{77}$$

The terms in the Reynolds stress equation (Equations (74) and (75)) and by extension that in the normalized Reynolds stress equation (Equation (76)) come from expanding the last term in the original OEC formulation (Equation (12)) and helps ensure the near-wall asymptotic behavior of the model. Note that D is often chose to be 2, thus eliminating the extra term in the R_{ij}*, which is desirable considering it can cause numerical difficulty near walls. E is chosen to be zero in an attempt to ensure that $\overline{q^2}$ (the average eddy vector magnitude) approaches a solid boundary like $(2/\alpha)/y^2$ where alpha is a tunable constant, usually set to $\alpha=15.0$. Note that OpenFOAM currently does not support tensors above rank two, and the implementation details of this term will be discussed later.

Implementing OEC in OpenFOAM

What is OpenFOAM?

The majority of the initial effort in this project focused on implementing the oriented eddy collision model in an open source collection of computational fluid dynamics libraries written in C++ called OpenFOAM. FOAM is unique in that much of the mathematical and numerical framework required to perform advanced CFD is already in place, available for any user to copy and modify for their own needs. Despite having a vast assortment of CFD-related tools, solvers, and utilities, the latest version of OpenFOAM (version 1.7.1 from OpenCFD LTD) has few Reynolds stress transport model implemented. In fact, it has only two: The Launder, Reece, and Rodi (1974) model and a variant, the Launder Gibson RSTM. Adding the OEC model to FOAM was not trivial, as no other model currently in FOAM must account for two to three transport equations for every eddy at every cell. This amounts to an entire collection of transport equations that must be carefully handled within FOAM, and is the first construct of its type to be implemented in FOAM. In its current form, OEC employs anywhere from 22 to over 1,200 eddies for simulations. The number of eddies available to the code is controlled by how the eddies may be arranged uniformly on a unit sphere.

```
fvm::ddt(qiINT)
- (1.0/3.0)*fvm::laplacian(dEff(), qiINT)
+ (1.0/3.0)*fvm::SuSp(((alpha*nu()*qsq + tauR)), qiINT)
==
- fvc::div(phi_, qiINT)
- ( qiINT & fvc::grad(U) )
- ( Ai + Bi )
```

Figure 28: FOAM provides a vast collection of operators to streamline the numerical side of implementing a turbulence model like OEC.

Figure 28 illustrates the power of OpenFOAM in that the software provides a wide variety of useful operators which eases the task of implementing a complex model such as OEC. The entry above constructs the evolution equation for q_i, and is contained within FOAM's "fvVectorMatrix" entity, the "fv" indicating "finite volume". Similar entities for tensors, "fvTensorMatrix" and scalars, "fvScalarMatrix" exist. All terms on the left hand side of the equation are cast implicitly, and are part of the matrix on the left hand side of the system to be solved which can be thought of as $\underline{\underline{A}}\,\underline{x} = \underline{b}$ with $\underline{\underline{A}}$ a rank two tensor (matrix) which must be inverted, $\underline{x}$ the vector of unknowns, and $\underline{b}$ the vector of known on the right hand side. Operators such as "fvm::ddt" easy to identify: "ddt" takes the time derivative of its argument, in this "qiINT" which is the eddy vector for the current eddy. Note that transport equations such as this are constructed for eddy vectors, Reynolds stress tensors, and in some cases the scalar kinetic energy for every eddy at every cell location in the computation mesh. In FOAM, "fvm::" casts the operator in the "finite volume method", which essentially places the operator (and resulting term) on the left hand (implicit) side of the equation, in $\underline{\underline{A}}$. For example, the Laplacian operator (used for the viscous diffusion term) is cast implicitly for stability purposes. The "SuSp" operator makes a decision about the location of the source term (and thus whether it is cast explicitly or implicitly, placed in $\underline{b}$ or $\underline{\underline{A}}$) based on its sign. Alternatively, operators may be cast using "fvc::", standing for "finite volume calculus", which is an explicit casting. This can be thought of as placing the resulting term in $\underline{b}$. For example, the convection term is handled with a call to "fvc::div", which performs an explicit divergence operation on the flux "phi_" and the eddy vector. The eddy vector production term $-q_k \overline{u}_{k,i}$ employs an explicit gradient operator (there is no such thing as an implicit gradient operator) along with FOAM's inner product, "&". Finally, explicit source terms such as the return-to-isotropy A_i and rotation term B_i, which are constructed beforehand, can simply be added directly to the equation.

Initial conditions for eddy vectors

A variety of initial conditions for the eddy vectors q_i and L_i are available for use with OEC. These initial conditions are in the form of a collection of vectors which are uniformly distributed on the unit sphere. These vector lists were originally created by Chartrand (2005) and have been adapted for use in OpenFOAM. The number of eddies employed in a given simulation is akin to the size of the statistical sampling space given to the underlying probability density function evolution equation underlying

the model. In theory, the more statistical sample space (eddies) given to the model, the better representation of the underlying physics is returned. This, however, comes at a cost, one which is brought to light as the details of implementing such a system in OpenFOAM are considered. Specifically, a system is required by which an *arbitrary* number of eddy vectors may be used in any given simulation. Based on the number of eddies (N), each cell in the computational domain must be populated with N Reynolds stress tensors, N eddy vectors, and N transport equations for each. In addition, model variants that employ the normalized stress tensor $R_{ij}^{*} \equiv R_{ij} / K$ require a third transport equation for the scalar kinetic energy. Two to three transport equations for each eddy at each physical location in the computational mesh (*i.e.*, at each cell) requires precise accounting. Pointer lists are employed for this purpose in FOAM. For some number of initial eddy vectors N, a pointer list with N entries is constructed for the eddy vectors themselves, for the corresponding Reynolds stress tensors, and if necessary for the scalar kinetic energy. A subtlety arises in this implementation, which will be discussed in the next section.

As mentioned above, the eddies are arranged on a unit sphere and are thus unit vectors. Considering the magnitude of the eddy vectors governs the dissipation, these vectors must be scaled before they are evolved and employed in the evolution of the Reynolds stress tensor. The initial eddy vectors are scaled by the positive root to the following quadratic equation (with roots β):

$$\left[\nu\frac{1}{N}\sum\left(\overline{q^2 k}\right)\cdot\alpha\right]\beta^2+\left[\left(K^0\right)^{\frac{3}{2}}\overline{|q_i|}\right]\beta=\frac{\left(K^0\right)^2}{\nu\,\mathrm{Re}_T{}^0} \tag{78}$$

with K^0 and $\mathrm{Re}_T{}^0$ the initial kinetic energy and turbulent Reynolds number, respectively. Setting the initial kinetic energy and turbulent Reynolds number in turn sets the initial desired length scale (or eddy vector magnitude), which can be thought of as the initial dissipation present in the flow under consideration. Note that the average eddy magnitude is calculated by

$$\overline{|q_i|}=\left[\frac{1}{N}\sum\left(q^2\right)\right]^{\frac{1}{2}} \tag{79}$$

where N is the number of eddies employed in a given simulation. For the model variants which employ the alternate length scale L_t (the "LR" and "LkR*" models), Equation (78) can be replaced by

$$\left[\nu\frac{1}{N}\sum\left(\overline{\left(\frac{1}{L^2}\right)K}\right)\cdot\alpha\right]\beta^2+\left[\frac{\left(K^0\right)^{\frac{3}{2}}}{\overline{|L_i|}}\right]\beta=\frac{\left(K^0\right)^2}{\nu\,\mathrm{Re}_T{}^0} \tag{80}$$

again noting that with $\overline{|L_i|} = \left[(1/N)\sum\left(L^2\right)\right]^{\frac{1}{2}}$ similar to Equation (79) above. The per-eddy Reynolds stresses are scaled by the user-set initial average Reynolds stress tensor $\overline{R_{ij}^0}$ once the eddy vectors have been properly scaled:

$$R_{ij}^{IC} = 3\left[\overline{R_{ij}^0} - \frac{q_i \cdot \left(\overline{R_{jk}^0} \cdot q_k\right)}{q^2} - \frac{q_j \cdot \left(\overline{R_{ik}^0} \cdot q_k\right)}{q^2} + \frac{q_s \cdot \left(\overline{R_{st}^0} \cdot q_t\right)}{q^2} \cdot \delta_{ij} - \left(\delta_{ij} - \frac{q_i q_j}{q^2}\right) \cdot \left(\frac{\overline{R_{kk}^0}}{2}\right)\right] \tag{81}$$

Again for the for the "LR" and "LkR*" variants, the initial Reynolds stresses are :

$$R_{ij}^{IC} = 3\left[\overline{R_{ij}^0} - L_i \cdot \left(\overline{R_{jk}^0} \cdot \frac{1}{L_k}\right) - L_j \cdot \left(\overline{R_{ik}^0} \cdot \frac{1}{L_k}\right) + L_s \cdot \left(\overline{R_{st}^0} \cdot \frac{1}{L_t}\right) \cdot \delta_{ij} - \left(\delta_{ij} - \frac{L_i L_j}{L^2}\right) \cdot \left(\frac{\overline{R_{kk}^0}}{2}\right)\right] \tag{82}$$

The turbulent Reynolds number Re_T^* is recalculated once it is employed for the initial eddy vector and stress tensor scaling:

$$\mathrm{Re}_T^* = \frac{\overline{K}^2}{\nu\varepsilon} = \frac{\overline{K}^2}{\nu\left[\frac{1}{N}\sum\left(q^2 K\right)\nu\alpha + \overline{K}^{\frac{3}{2}}\overline{|q_i|}\right]} \tag{83}$$

And for the "LR" and "LkR*" model variants:

$$\mathrm{Re}_T^* = \frac{\overline{K}^2}{\nu\varepsilon} = \frac{\overline{K}^2}{\nu\left[\frac{1}{N}\sum\left(\frac{K}{L^2}\right)\nu\alpha + \frac{\overline{K}^{\frac{3}{2}}}{\overline{|L_i|}}\right]} \tag{84}$$

The somewhat unusual form of the turbulent Reynolds number formulations in Equations (83) and (84) comes from the fact that the OEC model has no specific prescriptions for the dissipation ε, thus requiring the complex denominator.

Pointer lists

For every cell in a computational domain, there exists a collection of eddies in that cell. For every eddy, there is an associated eddy vector which has an evolution equation, an associated Reynolds stress tensor with an evolution equation, and a scalar kinetic energy which has an evolution equation if the "qkR*" or "lkR*" model variants are employed. This concept is illustrated in Figure 29:

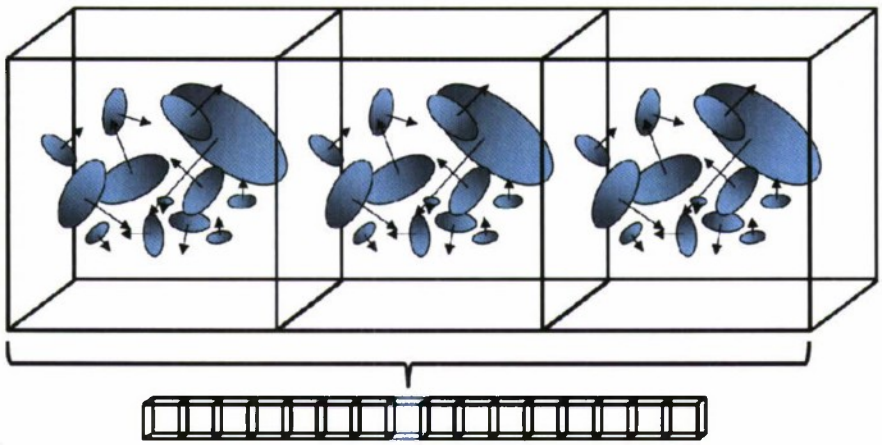

Figure 29: Schematic diagram of a collection of eddies that may exist in some turbulent flow. Note that each set of eddies exists at every cell in the computational mesh.

Three pointer lists, of length N (where N is the number of eddies originally seeded in the flow) are constructed. One is populated with FOAM's "volVectorField" entity, which stores a single vector at every cell location, responsible for handling the eddy orientation vectors. A second contains a "volSymmTensorField" array, which stores a six component symmetric tensor at every cell, handling the Reynolds stress tensor. The third (when needed) is a FOAM "volScalarField" which, not surprisingly, stores a scalar at every cell location, in this case containing the kinetic energy. The aforementioned subtlety comes when considering the way in which this information is accessed. Considering each pointer list entry is assigned to a specific eddy, operations performed across the entire computational domain are performed *one eddy at a time* because the pointer lists are iterated through on a *per-eddy* basis. To understand this, imagine selecting only the large, downward-pointing eddy in Figure 29 at every cell location and manipulating one of its associated quantities. The alternative of course it to pick one cell (perhaps the center cell in Figure 29) and select every eddy at that cell, manipulating some eddy's associated value at that cell alone. This has advantages and disadvantages. Accounting for the many, many tensors, vectors, and scalars in any given flow is trivial, as each pointer list is of size N, each entry corresponding to the kinetic energy for one eddy at each cell, one eddy orientation vector at each cell, or one eddy's Reynolds stress tensor at each cell. This makes performing averages over all eddies as simple as a summation over all pointer list entries and a division by N. This choice makes operations that must be performed on every eddy *at a given cell* much more difficult, however. Such operations are rare, but require extensive looping over each pointer list at each cell location, an expensive operation.

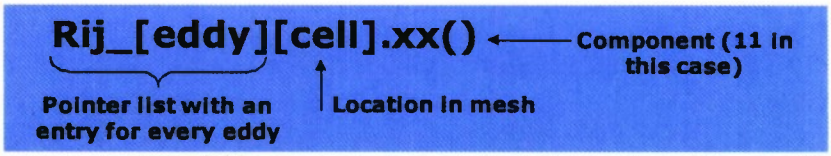

Figure 30: Using variable-sized pointer lists for per-eddy quantities in FOAM.

One of the most powerful and useful features of OpenFOAM is the ability to access and manipulate the components of a vector or tensor field across an entire mesh (*i.e.* across all cells and boundary patches) without the need to explicitly access each cell location. In fact, FOAM's namesake, *"field operation and manipulation"*, betrays the power of this ability and makes the implementation of such a complex model much simpler in C++. Unfortunately, this feature may only be used if access to one eddy's components across the entire computational domain is required, and not the opposite, where the component of all eddies at a single cell is required. In Figure 30, the pointer list addressing is illustrated. If it is sufficient to access a given eddy's components (or other associated entities, such as "correctBoundaryConditions", a function that updates or recalculates a field's boundary values) the cell addressing may be omitted altogether, greatly increasing the efficiency of all such operations.

Gradient of a rank two tensor

The evolution equations for both the "standard" and normalized Reynolds stress tensor, for both includes a term that involves the gradient of the Reynolds stress tensor, as shown in Equations (85) and (86). This is a rank two tensor, and its gradient produces a rank three tensor. Unfortunately, as of OpenFOAM 1.6, rank three tensors were not accommodated for. The templating was in place, but no operators could handle such an entity, including the gradient operator. As such, either an operator must be created that could return a rank three tensor, or a custom function written that could perform the calculation required in the model.

$$-D\left(\nu+\hat{\nu}_t\right)\left[\frac{R_{ij}}{K}\right]_{,k}(K)_{,k} \tag{85}$$

$$+(2-D)\left(\nu+\hat{\nu}_t\right)\left[R_{ij}^{*}\right]_{,k}\frac{(K)_{,k}}{K} \tag{86}$$

The first choice, extending the existing gradient operator to handle any rank two tensor would require immense effort (to make this operator sufficiently general and interface with the existing operator templates in OpenFOAM) and thus was deemed more effort than it was worth. The second option, writing a custom function to perform the desired gradient *in this model* was instead completed. Specifically, the function was created to calculate the inner product of the stress tensor gradient (a rank three tensor) and the gradient of the kinetic energy (a rank one tensor) which results in a rank two tensor. A code snippet from the function is provided in Figure 31:

```
forAll (mesh_.C(), cell)        // internal cells
 (
      Rx[cell].x() = Rtmp[cell].xx();
      Rx[cell].y() = Rtmp[cell].xy();
      Rx[cell].z() = Rtmp[cell].xz();
      ...
      gradKgradR[cell].xx() = ( gradK[cell].x()*gradRx[cell].xx()
                              + gradK[cell].y()*gradRx[cell].xy()
                              + gradK[cell].z()*gradRx[cell].xz() );
      gradKgradR[cell].yy() = ( gradK[cell].x()*gradRy[cell].yx()
                              + gradK[cell].y()*gradRy[cell].yy()
                              + gradK[cell].z()*gradRy[cell].yz() );
      gradKgradR[cell].zz() = ( gradK[cell].x()*gradRz[cell].zx()
                              + gradK[cell].y()*gradRz[cell].zy()
                              + gradK[cell].z()*gradRz[cell].zz() );
```

Figure 31: An example of the custom function written for calculating the gradient term from Equations (85) and (86). Note that looping over all cell locations may be avoided in circumstances when

Future work on OEC in OpenFOAM may include the creation of a template, generic gradient operator that can take a rank two tensor as an input and return a rank three tensor.

The PISO loop

Most non-steady state solvers in OpenFOAM use the so-called pressure implicit with splitting of operators ("PISO") loop to correct the pressure term, details of which can be found in Ferziger and Perić (2002), Anderson (1995), Rusche (2002) and Jasak (1996). The basic algorithm is contained within many OpenFOAM solvers and is augmented with equations from Ferziger and Perić (2002), Rusche (2002) and Jasak (1996). To begin with, the momentum equation is constructed keeping in mind that the flux (of the velocity) is treated explicitly using the last known value of the velocity. The momentum equation is then solved using the last known value of pressure on the right hand side. This results in a velocity field that is not divergence free, but approximately satisfies momentum. The velocity at some node P is obtained by solving the linearized momentum equation (Ferziger and Perić 2002):

$$A_P^{u_i} u_{i,P}^{m^*} + \sum_l A_l^{u_i} u_{i,l}^{m^*} = Q_{u_i}^{n+1} - \left(\frac{\partial p^{m-1}}{\partial x_i} \right)_P \tag{87}$$

and is expressed as (Ferziger and Perić 2002):

$$u_{i,P}^{m^*} = \frac{Q_{u_i}^{m-1} - \sum_l A_l^{u_i} u_{i,l}^{m^*}}{A_P^{u_i}} - \frac{1}{A_P^{u_i}} \left(\frac{\partial p^{m-1}}{\partial x_i} \right)_P \tag{88}$$

with $Q_{u_i}^{m-1}$ the collection of source terms that can be computed using velocity at time $m-1$ in terms of the velocity u_i^{m-1} (where the superscript m in u_i^m is the current estimate to the solution to the velocity u_i^{n+1} at time $n+1$) and l denoting the neighboring points

from the momentum equation discretization. $A_l^{u_i}$ contains the coefficients based on the old u_i at neighboring node(s) l, while $A_P^{u_i}$ is the same for the current node in question. $u_{i,P}^{m^*}$ and $u_{i,l}^{m^*}$ represent the current solution to the velocity at the node in question and surrounding nodes, respectively, and the * is meant to indicate that current solution is not the final solution and therefore does not satisfy the continuity equation.

After the momentum equation is set up and solved, the PISO loop begins and performs a given number of corrector loops. First, from the last solution of velocity, the diagonal terms are extracted from the matrix and the reciprocal is calculated and saved. Then, a Jacobi pass is taken and the velocity updated (see Jasak 1996 and Rusche 2002). The fluxes are then calculated accounting for the divergence of the velocity field by removing the difference between the interpolated velocity and the flux. The inlet and outlet fluxes are then adjusted to obey continuity Finally, if requested by the FOAM user, another loop begins (inside of the main PISO loop) which iteratively corrects for non-orthogonality. This step ends the main PISO loop. From there, the pressure gradient is added to the velocity field, noting that the pressure is the entire pressure field, not a correction. To summarize the algorithm (adapted from Ferziger and Perić 2002):

- To begin with, calculate fields at time t_{n+1} at some node i using values u_i^n and p^n as the initial guess for u_i^{n+1} and p^{n+1}.
- Build and solve the linearized momentum equation for $u_i^{m^*}$.
- Solve the pressure correction equation to obtain the intermediate pressure.
- Correct the velocity u_i^m and pressure p^m such that satisfy the continuity equation.
- Repeat this procedure updating u_i^m and p^m to iteratively improve estimates for u_i^{n+1} and p^{n+1} until the corrections become small.
- Finally, advice in time.

Note that this method is an alternative to very popular fractional step methods, which have been employed in previous implementations of OEC.

Implementation details concerning solid boundaries

Eddies that lie close to or on a wall are rotated such that they are not embedded in the wall. For a given eddy vector q_i, the following transformation is applied until the

eddy has been rotated far enough from the wall making sure that the magnitude of $\hat{q}_i$ remains unchanged:

$$q_i = \gamma \left[q_i - \chi \begin{pmatrix} q_1 \\ 0 \\ q_3 \end{pmatrix} \right] \tag{89}$$

With the scalar coefficients

$$\chi = 1 - \frac{y_{cell}}{\left({q_1}^2 + {q_3}^2 \right)^{\frac{1}{2}}} \tag{90}$$

and

$$\gamma = \left[\frac{|q_i|^2}{\left(1-\chi^2\right)\left({q_1}^2 + {q_3}^2\right) + {q_2}^2} \right]^{\frac{1}{2}} \tag{91}$$

where y_{cell} is the distance of the eddy in question from the nearest wall. Note once again that the hats have been dropped for convenience. The loop terminates when $|a_i|^2 \le {y_{cell}}^2$ where $a_i = q_i \times n_i$ and n_i is the unit normal vector of the nearest wall. The same procedure works if L_i is substituted for q_i. Once an eddy is rotated, the corresponding Reynolds stress tensor must also be rotated in order to ensure q_i and R_{ij} remain orthogonal. Rodrigues' rotation formula is employed:

$$T_{ij} = P_{ij} + (\delta_{ij} - P_{ij}) \cos\phi + L_{ij} \sin\phi \tag{92}$$

with ϕ the angle between the original and rotated eddy vector, the cosine between the old and new vectors is defined as $\cos\phi = \left({q_i}^{old} \cdot q_i \right) / \left(\left| {q_i}^{old} \right| |q_i| \right)$, and the sine subsequently calculated via $\sin\phi = \sqrt{1 - \cos^2\phi}$, and $P_{ij} = a_i a_j$. The skew-symmetric tensor L_{ij} is defined for each as

$$L_{ij} = \begin{bmatrix} 0 & -a_3 & a_2 \\ a_3 & 0 & -a_1 \\ -a_2 & a_1 & 0 \end{bmatrix} \tag{93}$$

Finally, employing Equation (92) above, R_{ij} is rotated via $R_{ij} = T_{ji} R_{ij} T_{ij}$. The same procedure works if L_i is substituted for q_i. Several ideas are implicit to this selection of a near wall rotation algorithm. First, and most importantly, the procedure outlined above does not alter the magnitude of the eddy vector it is operating on. This essentially decouples the near wall dissipation from the rotation operation. Whether this is physical or not is still the subject of current research. It may be the case that

such near wall realignment does in fact affect the dissipation and thus should affect the magnitude of the eddy vectors. Independent of the magnitude of the eddy vectors, the Reynolds stress tensor rotation must conserve kinetic energy both locally and globally, as it is surmised that eddy realignment (at least realignment that does not affect the eddy vector magnitude) should not affect the local or global kinetic energy. The method used to rotate the per-eddy stress tensors conserves local kinetic energy (*i.e.* the trace of the stress tensor remains constant) and validation cases have shown that global kinetic energy (the trace of the average stress tensor) is also preserved.

For the most part, eddies have at least two non-zero components and theory associated orientation vectors are neither perfectly normal to nor tangent to a solid boundary, as illustrated in Figure 32 A. Figure 32 B illustrates two troublesome situations. On the left, the eddy is perfectly tangential to the wall and on the right the eddy is perfectly normal to the wall. The above rotation algorithm fails in these situations. If the eddy is normal, the eddy should never be rotated as it cannot be

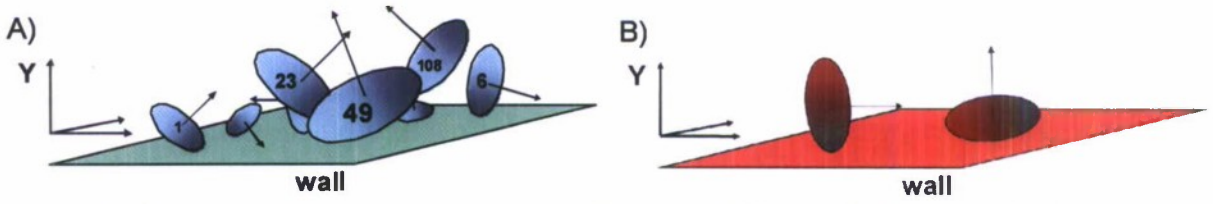

Figure 32: A) Most eddies are not aligned tangential or normal to a solid boundary. B) Some eddies lay be normal to (left) or tangential to (right) a wall.

intersecting the wall. This is case rarely, but must be accommodated. In the event of a perfectly parallel eddy, the problem becomes more serious. In this case, the normal component of the eddy vector (in this case, the Y components) is identically (or close to) zero. Even if the eddy is embedded in a wall (see Figure 26), the algorithm above will fail. Either it will fail to rotate the eddy (as no changed to the tangential X or Z components can possibly rotate the eddy away from the wall) or it will spin the eddy about its wall-normal (Y) axis forever. Neither case is desirable, as the eddy must be rotated out of the wall but the standard approach will not work. Several possible solutions exist, including "nudging" the eddy away from the wall by forcing the wall-normal (Y) component to be non-zero. Of course, the sign of the arbitrary non-zero Y component will dictate whether the resulting eddy vector points toward or away from the wall. There is no correct answer to this question, and as of now the OEC near-wall algorithm chooses to point all perfectly-tangential eddies slightly away from the solid boundary they are embedded in to.

Moving from the region near a solid boundary to the wall itself, the boundary conditions imposed on the eddy vectors and Reynolds stress tensor will be discussed. Two types of solid boundaries will be considered: first, a classic "slip" wall where surface-normal velocities are forced to zero (a no-penetration condition) but tangential components are undamped, that is a zero gradient condition is set as the boundary condition. The appropriate boundary conditions for velocity are obvious, as are those for other quantities such as kinetic energy, pressure, and so on. Appropriate boundary

conditions for the eddy vectors and Reynolds stress tensors are less obvious, however. Equation (94) proposes slip wall boundary conditions for the Reynolds stress tensor R_{ij}

$$R_{ij}\Big|_{slip-wall} = \begin{bmatrix} \frac{\partial R_{11}}{\partial y} = 0 & R_{12} = 0 & \frac{\partial R_{13}}{\partial y} = 0 \\ & R_{22} = 0 & R_{23} = 0 \\ & & \frac{\partial R_{33}}{\partial y} = 0 \end{bmatrix} \tag{94}$$

And for the original eddy vectors q_i:

$$q_i\Big|_{wall} = \begin{bmatrix} q_1 = 0 \\ \frac{\partial q_2}{\partial y} = 0 \\ q_3 = 0 \end{bmatrix} \tag{95}$$

In Equation (94), all the components of the stress tensor which involve a vertical (2) component are set to zero, while those independent of the vertical component are set to zero gradient in the vertical (in this case, Y) direction. A different idea is applied to the eddy vectors in Equation (95). At a slip wall (indeed at any solid boundary), only the vertical component of the eddy vector is allowed grow or shrink (once again assuming Y is the wall-normal direction), and the two tangential components of the eddy vector are forced to zero. Selecting tensor components to be no-slip or zero gradient *in a certain direction* is somewhat nebulous in OpenFOAM. A boundary condition does exist which allows certain components of a vector or tensor to have zero gradient boundary conditions applied while others can have a fixed value (*i.e. zero*) condition applied. The current implementation of this boundary condition does not, however, allow for a zero gradient boundary condition *in a certain direction* to be applied – the zero gradient is applied to all directions of a given component.

The second case considered is somewhat simpler, that is appropriate boundary conditions at a no-slip wall (which is often of most interest to engineers) where most quantities are forced to zero. Again, many boundary conditions are obvious: all three velocity components are forced to zero, the kinetic energy is forced to zero as are all six components of the Reynolds stress tensor. The eddy vector q_i is left in the form of Equation (95) above, whereas all components of the eddy vector L_i are set to zero at the solid boundary, essentially forcing all eddies at the wall to be of zero size, which is intuitive physically. The prescription of such boundary conditions, while convenient in the case of a no-slip wall, causes several numerical issues that must be taken in to consideration. Specifically, forcing the eddy vectors L_i to be zero at solid boundaries can lead to unexpected behavior (in the form of divide-by-zeros) unless care is taken when implementing terms that include L_i or L^2 in the denominator.

Accomplishments

The Oriented Eddy Collision model has advanced significantly from its original form. The model has been tuned and tested with a variety of fundamental turbulent flows. The model has been parallelized, and implemented in OpenFOAM. Furthermore, extensive research in to the model's behavior near solid boundaries has been performed. To summarize:

- OEC has been implemented in an unstructured, fully three-dimensional, parallel Navier-Stokes code (OpenFOAM).
- OEC has been validated and tested in FOAM using previously employed benchmarks as well as several new test cases.
- Feasible boundary conditions have been developed for use on slip and no-slip boundaries.
- Insight has been gained in to the physical behavior of turbulent eddies near solid boundaries, and ways in which other Reynolds-stress transport models may be handled in such physical situations.
- The number of model constants present in the code has been reduced.
- OEC is in a position to be used by a wide audience for a variety of both fundamental and real-world turbulent flows.

Future Work

The Oriented Eddy Collision model is still under development. Specifically, the behavior of the model near solid boundaries is still being investigated and perfected. Future work may include:

- Using OEC in OpenFOAM to determine the model's ability to predict turbulent transition.
- Continuing to test and perfect the model's behavior near solid boundaries.
- Extending the FOAM cases to flows of interest to engineers.
- Optimizing OEC's performance in OpenFOAM.

References

Wigeland, R.A. and Nagib, H. M. Effects of rotation on decay of turbulence. Bull. Amer. Phys. Soc. **23**, pp 998, 1978.

L. Jacquin, O. Leuchter, C. Cambonxs and J. Mathieu. Homogeneous turbulence in the presence of rotation. Journal of Fluid Mechanics, **220**, pp 1-52, 1990.

G. Winckelmans, H. Jeanmart, D. Carati, On the comparison of turbulence intensities from large-eddy simulation with those from experiment or direct numerical simulation, Phys. Fluids **14**, 1809-1811, 2002.

S. B. Pope, Turbulent Flows, Cambridge University Press, 2000.

J.H Ferziger and M. Perić, Computational Methods for Fluid Dynamics, Springer Press, New York, 2002.

Matsumoto, A., Nagano, Y. and Tsuji, T., "Direct Numerical Simulation of Homogeneous Turbulent Shear Flow," 5th Symposium on Computational Fluid Dynamics, pp. 361-364, 1991.

O. Reynolds. On the dynamical theory of incompressible viscous fluids and the determination of the criterion. Philosophical Transactions of the Royal Society of London A,186:123–164, 1895.

L. Prandtl. Bericht uber Untersuchungen zur ausgebildeten Turbulenz. Z. angew. Math. Mech., 5:136–139, 1925.

L. Prandtl. Uber ein neues Formelsystem fur die ausgebildete Turbulenz. Nachr. Akad. Wiss. Gottingen, pages 6–19, 1945.

W.C. Reynolds. Computation of Turbulent Flows. Annual Review of Fluid Mechanics, 8:183–208, 1976.

B. Baldwin and H. Lomax. Thin-layer approximation and algebraic model for separated turbulent flows. American Institute of Aeronautics and Astronautics, Aerospace Sciences Meeting, 1978.

P.R. Spalart and S.R. Allmaras. A one-equation turbulence model for aerodynamic flows. La Recherche Aerospatiale, 1(1):5–21, 1994.

P.A. Durbin and B.A. Pettersson Reif. Statistical Theory and Modeling for Turbulent Flows. John Wiley and Sons, New York, NY, USA, 2001.

W.P. Jones and B.E. Launder. The prediction of laminarization with a two-equation model of turbulence. International Journal of Heat and Mass Transfer, 15(2):301–314, 1972.

D.C. Wilcox. Turbulence Modeling for CFD. DCW Industries, La Canada, CA, USA, 1993.

D.C. Wilcox. Re-assessment of the scale-determining equation for advanced turbulence models. AIAA Journal, 26:1414–1421, 1988.

D.B. Spalding. Kolmogorov's two-equation model of turbulence. Proceedings of the Royal Society of London A, 434:211–216, 1991.

A.N. Kolmogorov. Equations of turbulent motion of an incompressible fluid. Izv. Akad. Nauk SSSR, Seria fizicheska VI, (1-2):56–58, 1942.

T.J. Craft, B.E. Launder, and K. Suga. Development and application of a cubic eddy-viscosity model of turbulence. International Journal of Heat and Fluid Flow, 17:108–115, 1996.

P.A. Durbin. Separated Flow Computations with the $k-\epsilon-v^2$ Model. AIAA J, 33(4):659–664, 1995.

J. Rotta. Statistische Theorie nichthomogener Turbulenz. Zeitschrift für Physik A Hadrons and Nuclei, 129:547–572, 1951.

J. Gadebusch. On the development of self-adapting (RANS/LES) turbulence models for fluid simulation at any mesh resolution. Master's thesis, The University of Massachusetts, Amherst, 2007.

J.B. Perot and J. Gadebusch. A stress transport equation model for simulating turbulence at any mesh resolution. Theoretical and Computational Fluid Dynamics, 23:271–286, 2009.

S.B. Pope. Consistent modeling of scalars in turbulent flows. Physics of Fluids, 26(2):404–408, 1982.

S.B. Pope. A Lagrangian two-time probability density function equation for inhomogeneous turbulent flows. Physics of Fluids, 26(12):3448–3450, 1983.

S.B. Pope. Lagrangian PDF methods for turbulent flows. Annual Review of Fluid Mechanics, 26:23–63, 1994.

S.B. Pope. Turbulent Flows. Cambridge University Press, New York, NY, USA, 2000.

T.S. Lundgren. Distribution Functions in the Statistical Theory of Turbulence. Physics of Fluids, 10(5):969–975, 1967.

P.R. Van Slooten and S.B. Pope. PDF modeling for inhomogeneous turbulence with exact representation of rapid distortions. Physics of Fluids, 9(4):1085–1105, 1996.

G.I. Taylor. Diffusion by continuous movements. Proceedings of the London Mathematics Society, 20:196–212, 1921.

G.I. Taylor. Statistical theory of turbulence. Proceedings of the Royal Society of London. Series A, Mathematical and Physical Sciences, 151(873):421–444, 1935.

H. Tennekes and J.L. Lumley. A First Course in Turbulence. Cambridge, Massachusetts,1972.

M. Martell. Simulations of turbulence over superhydrophobic surfaces. Master's thesis, The University of Massachusetts, Amherst, 2009.

L.F. Richardson. Weather Prediction by Numerical Process. Cambridge University Press, Cambridge, UK, 1922.

D.C. Haworth and S.B. Pope. A generalized Langevin model for turbulent flows. Physics of Fluids, 29(2):387–405, 1985.

W.C. Reynolds and S.C. Kassinos. One-point modeling of rapidly deformed homogeneous turbulence. Proceedings of the Royal Society of London A, 451:87–104, 1995.

C.G. Speziale. Analytical methods for the development of Reynolds-stress closures in turbulence. Annual Review of Fluid Mechanics, (23):107–157, 1991.

D.S. Lemons and A. Gytheil. Paul Langevin's 1908 paper: On the Theory of Brownian Motion . The American Journal of Physics, 65 (11):1079–1081, 1997.

J. Boussinesq. Théorie de l'écoulement tourbillant. Mem. Presentes par divers Savants Acad. Sci. Inst. Fr., 23:46–50, 1877.

E.R. van Driest. On Turbulent Flow Near a Wall. Journal of the Aeronautical Sciences, 23(11):1007–1011, 1956.

J. Smagorinsky. General circulation experiments with the primitive equations. Monthly Weather Review, 91(3):99–164, 1963.

P.R. Spalart. Strategies for turbulence modeling and simulations. International Journal of Heat and Fluid Flow, 21:252–263, 2000.

P.G. Saffman. A Model for Inhomogeneous Turbulent Flow. Proceedings of the Royal Society of London A, 317:417–433, 1970.

P.G. Saffman and D.C. Wilcox. Turbulence-Model Predictions for Turbulent Boundary Layers, 1974.

B.E. Launder and D.B. Spalding. Mathematical Models of Turbulence. London, 1972

D.C. Wilcox and I.E. Alber. A Turbulence Model for High Speed Flows. Proc. of the 1972 Heat Trans. & Fluid Mech., pages 231–252, 1972.

D.C. Wilcox. Reassessment of the Scale Determining Equation for Advanced Turbulence Models. AIAA Journal, 26 (11):1299–1310, 1988.

C.G. Speziale. On nonlinear $k-l$ and $k-w^2$ models of turbulence. Journal of Fluid Mechanics, 178:459–475, 1987.

B.E. Launder, G.J. Reece, and W. Rodi. Progress in the development of a Reynolds- stress turbulence closure. Journal of Fluid Mechanics, 68 (3):537–566, 1974.

C.G. Speziale, S. Sarkar, and T.B. Gatski. Modeling the pressure strain correlation of turbulence: an invariant dynamical systems approach. Journal of Fluid Mechanics, (227):245–272, 1991.

J.B. Perot and C. Chartrand. Modeling return to isotropy using kinetic equations. Physics of Fluids, 17:035101–1:035101–18, 2005.

C.C. Chartrand. Eddy Collision Models for Turbulence. Master's thesis, The University of Massachusetts, Amherst, 2005.

W. Chang, F. Giraldo, and J.B. Perot. Analysis of an Exact Fractional Step Method. Journal of Computational Physics, 179:1–17, 2002.

J.L. Lumley. Computational Modeling of Turbulent Flows. Advances in Applied Mechanics, 18:123–176, 1978.

C.G. Speziale. Turbulence Modeling in Non-inertial Frames of Reference. Theoretical and Computational Fluid Dynamics, 1:3–19, 1989.

P.R. Spalart and C.G. Speziale. A note on constraints in turbulence modeling. Journal of Fluid Mechanics, 391:373–376, 1999.

C.duP. Donaldson and H. Rosenbaum. Calculation of the turbulent shear flows through closure of the Reynolds equations by invariant modeling. Aeronautical Research Association Princeton, Princeton, NJ, (127):0–1, 1968.

U. Schumann. Realizability of Reynolds-stress turbulence models. Physics of Fluids, 20(5):721–725, 1977.

J.L. Lumley. Computational Modeling of Turbulent Flows. Advances in Applied Mechanics, 18:123–176, 1978.

M.B. Martell, J.B. Perot, and J.P. Rothstein. Direct numerical simulations of turbulent flows over superhydrophobic surfaces. Journal of Fluid Mechanics, 620:31–41, 2009.

M.B. Martell, J.P. Rothstein, and J.B. Perot. An analysis of superhydrophobic turbulent drag reduction mechanisms using direct numerical simulation. Physics of Fluids, 22:065102:1–13, 2010.

S.M. de Bruyn Kops and J.J. Riley. Direct numerical simulation of laboratory experiments in isotropic turbulence. Physics of Fluids, 10:2125–2127, 1998.

S.M. de Bruyn Kops, J.J. Riley, and G. Kos'aly. Direct numerical simulation of reacting scalar mixing layers. Physics of Fluids, 13:1450–1465, 2001.

John Kim, Parviz Moin, and Robert Moser. Turbulence statistics in fully developed channel flow at low Reynolds number. Journal of Fluid Mechanics, 177:133–166, 1987.

R. Moser, J. Kim, and N. Mansour. Direct numerical simulation of turbulent channel flow up to Re_τ =590. Physics of Fluids, 11(4):943–945, 1998.

M. Nilsson. Exploring fundamental turbulent physics using direct numerical simulation. Master's thesis, The University of Massachusetts, Amherst, 2009.

M. Herrchen and H.C. O¨ ttinger. A detailed comparison of various FENE dumbbell models. Journal of Non-Newtonian Fluid Mechanics, 68(1):17 – 42, 1997.

J.G. Olroyd. On the Formulation of Rheological Equations of State. Proceedings of the Royal Society of London. Series A, Mathematical and Physical Sciences, 200(1063):523–541, 1950.

P.L. Bhatnagar, E.P. Gross, and M. Krook. A Model for Collision Processes in Gases. I. Small Amplitude Processes in Changed and Neutral One-Component Systems. Physical Review, 94(3):511–525, 1954.

R. Andeme. Development of an Oriented-eddy Collision Model for Turbulence. Master's thesis, The University of Massachusetts, Amherst, 2008.

J.B. Perot and S.M. de Bruyn Kops. Modeling turbulent dissipation at low and moderate Reynolds numbers. Journal of Turbulence, 7 (69):1–14, 2006.

R. S. Rogallo and P. Moin, Numerical simulation of turbulent flows, Annual Rev. Fluid Mech. 16, 99-137, 1984.

P. R. Spalart, Strategies for turbulence modeling and simulations, Engineering Turbulence Modelling and Experiments 4, Rodi and Laurence, eds. Elsevier, 1999.

M. Germano, Turbulence: the filtering approach, J. Fluid Mech,. 238, 325-336, 1992.

S.A Orzag, V. Yakhot, W.S. Flannery, F. Boysan, D. Choudhury, J. Marusewski and B. Patel, B., Renormalization group modeling and turbulence simulations", So, R.M.C., Speziale, C.G. and Launder, B.E. (eds.), Near-wall turbulent flows. Elsevier Science Publisher, 1993.

P.A. Durbin, Near-wall turbulence closure modeling without 'damping functions', Theoret. Comput. Fluid Dynamics 3, 1-13, 1991.

W. C. Reynolds, Effects of rotation on homogeneous turbulence, Proc. Of the 10th Australasian Fluid Mech. Conf. pp. 1-6, Melbourne, 1989.

A. Matsumoto, Y. Nagano and T. Tsuji, Direct Numerical Simulation of Homogeneous Turbulent Shear Flow, 5th Symposium on Computational Fluid Dynamics, pp. 361-364, 1991.

G. Compte-Bellot and S. Corrsin, Simple Eulerian time correlations of full and narrow-band velocity signals in grid generated isotropic turbulence, J. Fluid Mech., 48, 273-337, 1971.

Chasnov, J. R, "Decaying turbulence in two and three dimensions", Advances in DNS/LES, Greyden Press, Columbus, Ohio, 1997.

Mansour, N. N., & Wray, A. A., "Decay of isotropic turbulence at low Reynolds number", Phys. Fluids, 6 (2), 808-814, 1994.

Yu, H., Girimaji, S. S. & Luo, L.-S, "DNS and LES of decaying isotropic turbulence with and without frame rotation using a lattice Boltzmann method", J. Comput. Phys., 209, 599-616, 2005.

G. A. Blaisdell & K. Shariff, "Simulation and modeling of the elliptic streamline flow". Proceedings of the 1996 Summer Program, Center for Turbulence Research, NASA Ames/Stanford Univ., 443-446, 1996.

J. B. Perot and P. Moin, "A Near Wall Model for the Dissipation Tensor," Eleventh Australasian Fluid Mechanics Conference, Hobart, Tasmania, Australia, 13-18, 1992.

L. Le Penven, J. N. Gence, and G. Comte-Bellot, "On the Approach to Isotropy of Homogeneous Turbulence: Effect of the Partition of Kinetic Energy Among the Velocity Components", Frontiers in Fluid Mechanics, 1-21, 1985.

S. G. Saddoughi and S. V. Veeravalli, "Local isotropy in turbulent boundary layers at high Reynolds number," J. Fluid Mech. 268, 333 -372, 1994.

J. B. Perot and P. Moin, "Shear-Free Turbulent Boundary Layers, Part I: Physical Insights into Near Wall Turbulence," J. Fluid Mech. 295, 199-227, 1995.

J. B. Perot & P. Moin, "Shear-Free Turbulent Boundary Layers, Part 2: New concepts for Reynolds stress transport equation modeling of inhomogeneous flows," J. Fluid Mech. 295, 229-245, 1995.

S. Tavoularis and S. Corrsin, "Experiments in nearly homogeneous turbulent shear flow with a uniform mean temperature gradient. Part1," J. Fluid Mech. 104, 311-347, 1981.

M. Hallbäck, J. Groth & A. V. Johansson, "A Reynolds stress closures for the dissipation in anisotropic turbulent flows," 7th Symposium on Turbulent Shear Flows, Stanford University, August. 1989.

M. Hallbäck, J. Groth & A. V. Johansson, "An algebraic model for nonisotropic turbulent dissipation rate in Reynolds stress closures," Phys. Fluids, **2** (10), 1859-1866, 1990.

K. S. Choi and J. L. Lumley, "Turbulence and Chaotic Phenomena in Fluids," Proceedings of the IUTAM Symposium (Kyoto, Japan), edited by T. Tatsumi, North-Holland, Amsterdam, p. 267, 1984.

M. Yamamoto and C. Arakawa, "Study on the Pressure-Strain Term in Reynolds Stress models." Proceedings of the Eighth Symposium on Turbulent Shear Flows, Technical University of Munich, Munich, Germany, pp. III-17-1 – III-17-2, 1991.

Jasak, H. Error Analysis and Estimation for the Finite Volume Method with Applications to Fluid Flows. PhD dissertation, Imperial College of Science, Technology and Medicine, 1996.

R.I. Issa, "Solution of the implicitly discretised fluid flow equations by operator-splitting," Journal of Computational Physics **62**, (1), pp. 40-56, 1986.

J.R. Anderson. Computational Fluid Dynamics – The Basics with Applications. McGraw-Hill, New York, 1995.

H. Rusche, Computational fluid dynamics of dispersed two-phase flows at high phase fractions, Imperial College of Science, Technology and Medicine, 2002.